THE NANOPOROUS MORPHOLOGY OF PHOTOPOLYMERIZED CROSSLINKED POLYACRYLAMIDE HYDROGELS

A Dissertation

by

JIAN WANG

Submitted to the Office of Graduate Studies of
Texas A&M University
in partial fulfillment of the requirements for the degree of

DOCTOR OF PHILOSOPHY

May 2008

Major Subject: Chemical Engineering

THE NANOPOROUS MORPHOLOGY OF PHOTOPOLYMERIZED CROSSLINKED POLYACRYLAMIDE HYDROGELS

A Dissertation

by

JIAN WANG

Submitted to the Office of Graduate Studies of
Texas A&M University
in partial fulfillment of the requirements for the degree of

DOCTOR OF PHILOSOPHY

Approved by:

Chair of Committee,	Victor M. Ugaz
Committee Members,	Zhengdong Cheng
	Terry Creasy
	Arul Jayaraman
Head of Department,	Michael Pishko

May 2008

Major Subject: Chemical Engineering

ABSTRACT

The Nanoporous Morphology of Photopolymerized Crosslinked Polyacrylamide Hydrogels. (May 2008)

Jian Wang, B.S., China University of Petroleum, Beijing, China;

M.S., Research Institute of Petroleum Processing

Chair of Advisory Committee: Dr. Victor M. Ugaz

Nanoporous polymer hydrogels offer a desirable combination of mechanical, optical, and transport characteristics that have placed them at the core of a variety of biomedical technologies including engineered tissue scaffolds, substrates for controlled release of pharmaceutical compounds, and sieving matrices for electrophoretic separation of DNA and proteins. Ultimately, we would like to obtain a detailed picture of the nanoscale pore morphology and understand how it can be manipulated so that we can rationally identify gel formulations best suited for a specific application. But this goal has proven elusive because the most fundamental descriptors of the pore network architecture (e.g., the average pore size and its polydispersity) are particularly difficult to measure in polymer hydrogels.

Here we introduce an approach that enables both the mean pore size and the pore size distribution to be quantitatively determined without prior knowledge of any physical material parameters A novel technique to prepare TEM samples was developed so that the nanoscale hydrogel pore size, pore shape and distribution are clearly visualized and

quantitatively studied for the first time. The pore sizes of the hydrogel are also estimated with rheology. A new fixture is used in the rheometer and the whole polymerization process can be directly studied using an in-situ rheology experiment. A series of thermoporometry experiments are also conducted, and suitable methods and equations to study hydrogel pore size and distribution are chosen. The pore size derived from TEM, rheology, DSC is compared and their values are self-consistent. These techniques help us understand how the nanoporous morphology of crosslinked polyacrylamide hydrogels is influenced by their chemical composition and polymerization conditions.

It is interesting to find hydrogels with similar pore size but different distribution. For two hydrogels with similar pore size, the broader the distribution, the faster the release rate and the higher the accumulated release percentage. So we can control the release of trapped molecules by simply varying the hydrogel pore size distribution. This discovery would have a very promising potential in the application of pharmaceuticals.

To my parents

To my wife Yu Pei

To my brother Yue Wang, and my sister Yuan Wang

ACKNOWLEDGEMENTS

First, I would like to thank my advisor Dr. Ugaz for introducing me to the field of polymer, especially hydrogels and rheology, and also for his guidance, support, patience and kindness during my research. He is my personal role model not only as an engineer but also as a person. The success of this work would not be possible without his guidance and help.

Second I would also like to thank my committee members, Dr. Zhengdong Cheng, Dr. Arul Jayaraman and Dr. Terry Creasy. I would especially like to thank Dr. Bevan for being on my committee and for the use of the rheometer when he was at Texas A&M University. I would like to express my gratitude to Dr. Zhiping Luo and E. Ann Ellis in the Microscopy and Imaging Center at Texas A&M University for their invaluable assistance with the TEM measurements. I also thank Rodney Inmon and Prof. Dimitris Lagoudas in the Materials and Structures Lab, as well as Prof. Hung-Jue Sue in the Polymer Technology Center for assistance with and use of the DSC instruments.

Finally, I would like to dedicate my Ph.D degree to my parents for their influence and unconditional love. I thank my wife for her love, encouragement, understanding and support. Every bit of my progress comes with their deep love.

TABLE OF CONTENTS

Page

LIST OF FIGURES

FIGURE Page

FIGURE Page

LIST OF TABLES

1. INTRODUCTION

Nanoporous polymer hydrogels have become indispensable in biomedical applications ranging from controlled release of pharmaceutical compounds[1, 2], to engineered tissue scaffolds[3, 4], to separation of DNA and proteins[5]. All the applications are closely related to the nanoporous morphology of the matrix, especially the mean pore size and its distribution.

Hydrogels are widely used in controlled release as they are able to swell in the presence of water or biological fluid causing the gel pore size (linear distance between the active junctions or crosslinks) to increase during the process. Thus the drug compounds previously trapped in the polymer matrix can be released or diffuse out of the gel at a constant rate over a long period of time. For example, poly(ethylene glycol) (PEG) is used to expand the lifetime of proteins and their release kinetics by coupling with proteins[6]. The trapped proteins can be protected and their release kinetics be well controlled by the gel matrix. Another example is Poly (vinyl alcohol) (PVA), which can be prepared by a freezing/thawing process and used as bioadhesive material to control the release kinetics. The hydrogel's mucoadhesive characteristics and drug release properties can be optimized by controlling the freezing/thawing conditions[7]. Acrylamide

This dissertation follows the style and format of *Nature Biotechnology*.

based hydrogels such as N-(2-hydroxypropyl) methacrylamide (HPMA) copolymers are unique for their electric neutrality and can be applied to control the drug release in tumor treatment using photodynamic therapy (PDT) because they are structurally diverse and can be modified to exhibit a range of subcellular accumulation levels and incorporate different covalent attachments of photosensitizers[8, 9] .

Hydrogels have also been developed for use in tissue engineering as three dimensional extracellular scaffolds that mimic the properties of natural extracellular matrices (ECM). The porous morphology of hydrogels gives them tissue like viscoelatic properties with similar diffusive transport and interstitial flow characteristics in the matrix as the ECM. These distinctive physiochemical features provide cells with a similar microenvironment that closely mimics in-vivo conditions. For example, polyethylene oxide (PEO) hydrogels can be synthesized by combining commercially available PEO macromers with cysteine-containing peptides under mild conditions[10, 11].These hydrogels have the great advantage of resisting nonspecific binding of biological macromolecules and provide an ideal base molecular scaffold that can be further modified by specific binding of adhesion molecules, growth-factor binding sites, and other moieties.

Many genomic assays involve biochemical reactions that generate populations of DNA fragments of varying size, after which product analysis is performed using gel

electrophoresis to ascertain the size and quantity of fragments present. This fractionation process relies on the ability to induce a size dependent mobility of negatively charged DNA molecules in the presence of an applied electric field. By constraining electrophoretic migration to occur through a gel matrix, interactions with the porous network introduce a size dependent mobility as smaller fragments experience less resistance and therefore are eluted more quickly than larger fragments. The physics of this migration process is critically dependent on the mean gel pore size and its distribution (average pore sizes of 5 – 10 nm are typical in single-stranded DNA sequencing applications). Crosslinked polyacrylamide is a widely used gel matrix for DNA electrophoresis because it offers a number of attractive properties including excellent separation resolution, optical/UV transparency, and electro-neutrality. In order to rationally engineer gels with properties that are optimally suitable for any of these applications, it is essential to understand the nature of the gel pore structure and parameters through which it can be manipulated.

Though the applications of hydrogels demand increasingly precise and reproducible control over the pore morphology, polymer hydrogels pose unique challenges that have frustrated efforts to obtain a detailed quantitative picture of their pore network architecture. Efforts to predict the average pore size and its distribution have proven challenging in hydrogel systems due to relatively complex polymerization

kinetics that involve side reactions such as cyclization and multiple crosslinking[12-15]. Experimental efforts to characterize these parameters have also been hampered by the underlying mechanical fragility and large amount of water present in the gels. Consequently, coordinated studies of the interplay between pore morphology, mechanical properties, and separation performance are lacking and at present the extent of morphological characterization is typically limited to coarse estimates of the mean pore size[16-18].

In this dissertation, we attempt to address this issue by employing a novel combination of a photoinitiated polyacrylamide / bis-acrylaimde polymerization chemistry and characterization techniques that have not been widely adapted to the study of hydrogel sieving matrices. First, we use in-situ dynamic small-amplitude oscillatory shear measurements performed during photopolymerization to investigate the influence of UV intensity, polymer composition, and reaction temperature on the mechanical properties of the hydrogel. A simple model based on classical rubber elastic theory then allows us to extract estimates of the average pore size that show good agreement with corresponding data obtained from analysis of DNA electrophoretic mobility.

Next, thermoporometry is employed to measure the melting point depression associated with water confined along the interior surfaces of the hydrogel pore network. This technique permits the average pore size and distribution to be determined, and is

especially suitable for use with fragile hydrogel samples.

Finally, we present a novel technique to prepare hydrogel samples at room temperature for direct visualization of nanoporous morphology using transmission electron microscopy (TEM). This new preparation technique virtually eliminates freeze fracture effects that often occur in standard preparation protocols and have made it difficult to image gel pore architectures without damaging them.

These techniques help us understand how the nanoporous morphology of crosslinked polyacrylamide hydrogels is influenced by their chemical composition and polymerization conditions. We then use these new insights to examine controlled release of macromolecules from these hydrogels and show that it is possible for gels to appear virtually identical when compared on the basis of their mean pore size, yet display remarkably dissimilar release kinetics owing to differences in polydispersity. The role of the pore size distribution has not been widely explored, but is likely to broadly influence the interplay between network structure, mechanical properties and transport characteristics in hydrogel systems.

2. RHEOLOGY OF PHOTOPOLYMERIZED CROSSLINKED POLYACRYLAMIDE HYDROGELS

2.1 Introduction

Crosslinked polyacrylamide hydrogels are typically synthesized by chemically initiated free radical co-polymerization of acrylamide and N, N'-methylene -bis-acrylamide (generally referred to as simply bisacrylamide or "bis").Ammonium persulfate (APS) is a commonly used initiator, in combination with TEMED (tetramethylethylenediamene) which catalyzes free radical formation in APS. These free radicals then associate with acrylamide monomers to begin polymerization, during which the growing polymer chains become chemically crosslinked through random incorporation of bis-acrylamide. In addition to chemical initiation, polymerization can also be driven by a photo-induced process whereby free radicals are generated by exposure to UV light. Interest in photopolymerization techniques has increased in recent years owing to their rapid polymerization times, enhanced control over reaction kinetics, reduced quantities of charged residues in the gel after polymerization, and the ability to tailor the gel structure by varying illumination intensity and exposure conditions. These capabilities are especially useful in the development of miniaturized electrophoresis systems because they allow hydrogel matrices to be precisely positioned at specific locations within a microfluidic network[19-24].

Studies of non-crosslinked acrylamide polymerization generally show good agreement with standard free radical kinetic models[25, 26]. Co-polymerization of crosslinked polyacrylamide hydrogels, however, involves a more complex interplay between growth of individual chains, crosslinking of neighboring chains, and intrachain cyclization. Each process is characterized by its own reaction pathway and rate constant, which in turn determines its contribution to the final gel pore structure. Efforts to study these effects experimentally date back to the seminal work of Gelfi and Righetti investigating the influence of crosslinker composition, polymerization temperature, and initiator chemistry[27-29]. Kinetic models of free radical crosslinking copolymerization have been developed to describe solution and gel properties in monovinyl-divinyl monomer systems, with predictions in good agreement with experimental data for copolymerization of styrene and m-divinylbenzene[30, 31]. Subsequent work has investigated free radical crosslinking polymerization of 1,4-divinylbenzene, where it was found that 60-80% of pendant vinyl groups were consumed by cyclization and that an average of 100 – 800 multiple crosslinks were formed for every single intermolecular crosslink[12]. In studies of acrylamide / bis-acrylamide copolymerization, the degree of cyclization was found to be as high as 80%, with average reactivity of pendant vinyl groups decreasing with increasing crosslinker concentration[13, 15]. Polymerization conditions such as temperature[32] and monomer

reactivity [33], as well as monomer concentration[34], crosslinker concentration[35], and swelling behavior[36] also influence the degree of homogeneity of the gel pore structure.

Rheology has emerged as an important gel characterization tool because in-situ experiments are relatively straightforward to perform during the polymerization process and because viscoelastic properties directly reflect the structure and morphology of the sample[37]. Klaveness et. al.[38] employed small amplitude oscillatory shear experiments to measure the storage (G') and loss (G'') moduli during crosslinking of polyacrylamide and Cr (III). These data were then used to characterize gelation kinetics in terms of a two-stage first-order process consistent with a description of crosslinking in terms of a parallel side reaction mechanism. Trompette et. al. [39] compared the rheological behavior of polyacrylamide and poly(sodium acrylate) hydrogels synthesized using an identical crosslinker and found that the magnitude of the complex shear modulus $|G^*|$ exhibited a different power law dependence on monomer concentration in the two systems. Most recently, Calvet et. al.[40] performed an extensive series of in-situ small amplitude oscillatory shear experiments during polymerization of polyacrylamide hydrogels using various crosslinker concentrations and reaction temperatures. Rubber elasticity theory was then used to extract a measure of the average network crosslink density and strand molecular weight. In addition to observing gelation kinetics, it was possible to identify

optimal crosslinker concentration and temperature conditions associated with a maximum in hydrogel elasticity (G'). These studies illustrate the ability of rheological techniques to identify appropriate polymerization conditions for synthesis of hydrogels incorporating desired microstructural properties.

Previous investigations of kinetics and rheology in polyacrylamide hydrogels have focused on chemically initiated polymerization reactions. Few, if any, comparable studies have been performed using UV initiated polymerization chemistries, despite their emerging importance. In addition to their practical application as sieving matrices for DNA electrophoresis, photopolymerized hydrogels offer several unique advantages as a platform for fundamental studies of polymerization kinetics. For example, their rapid polymerization times allow experiments to be performed in less than 30 minutes, as opposed to timescales of several hours in chemically initiated systems. In addition to the time savings, rapid polymerization is beneficial because problems associated with long experiment runs are greatly reduced (especially evaporation, which directly impacts a wide range of physical properties), leading to a higher degree of reproducibility. In addition, an enhanced level of control over the polymerization process can be exerted by manipulating the UV illumination. For example, the rate of free radical production can be increased or decreased (or even switched-off completely) at any time during the course of the reaction. This unique combination of properties

introduces the exciting possibility of tailoring the gel microstructure through direct control of the polymerization process.

In this session, we present a series of in-situ dynamic small amplitude oscillatory shear studies during photopolymerization of crosslinked polyacrylamide hydrogels. Using a parallel plate rheometer with an integrated UV illumination cell, we explore the influence of parameters including UV light intensity, monomer and crosslinker concentrations, and temperature during polymerization on the mechanical response of the resulting hydrogel. A simplified model based on classical rubber elasticity theory is then used to obtain estimates of the average gel pore size, which are compared to corresponding estimates derived from DNA mobility behavior during gel electrophoresis. This study illustrates the utility of rheological experiments as a tool to identify optimal conditions for synthesis of polyacrylamide hydrogels incorporating microstructural properties suitable for high-resolution electrophoresis of biomolecules under a variety of conditions.

2.2 Materials and experimental methods

2.2.1 Materials and hydrogel synthesis

Two different crosslinked polyacrylamide gel formulations were studied: (i) a commercial DNA sequencing gel (Long Ranger®; Cambrex Bio Science, Rockland, ME), and (ii) gels polymerized from solutions of powdered acrylamide and

bis-acrylamide with additives (Bio-Rad Laboratories, Hercules, CA). (iii) Crosslinked polyacrylamide hydrogels of simple formulations polymerized from solutions of powdered acrylamide, bis-acrylamide and APS as initiator without any other additives. Photopolymerizable LongRanger gel formulations were prepared by combining 60 µL of the appropriate dilution of gel stock solution in deionized water with 120 µL of the photoinitiator supplied with ReproGel® sequencing gels (Solution B; Amersham Biosciences Corp., Piscataway, NJ) and gently mixing to obtain final gel concentrations of 6, 9, and 12 %T.

Photopolymerizable formulations of gels from acrylamide and bis-acrylamide powder were prepared by combining monomer, crosslinker, and 7.2 g urea (a denaturant additive commonly used in DNA electrophoresis) in deionized water to make a total volume 16 mL. A 4 mL volume of 10x Tris-Borate-EDTA (TBE) electrophoresis buffer (Extended Range TBE Buffer; Bio-Rad Laboratories, Hercules, CA) was then added to bring the total volume to 20 mL (6 M final urea concentration). Immediately before each experiment, 3 µL of a freshly prepared (10% w/v) aqueous ammonium persulfate (APS) solution was added to 2 mL of the gel stock solution, along with 2.5 µL of a (0.4 % w/v) aqueous riboflavin solution to serve as a photoinitiator (APS and riboflavin powders were obtained from Bio-Rad Laboratories, Hercules, CA). A series of experiments were also performed using variable riboflavin

concentrations in a 9 %T gel stock solution. Finally the photoinitiator Irgacure 651 (Ciba Specialty Chemicals Corp., Tarrytown, NY) was also investigated. Here, 100 mg of Irgacure powder was dissolved in 5 mL of ethanol (Fisher Scientific, Pittsburgh, PA) to obtain a 2 % w/v solution, after which 3 μL of the Irgacure mixture was added to 2 mL of a 9 %T gel stock solution.

Crosslinked polyacrylamide hydrogels polymerized from simple formulations were polymerized from a solution of powdered acrylamide monomer and bis-acrylamide crosslinker with ammonium persulfate (APS) as the initiator. Stock solutions of photopolymerizable gel formulations were prepared by combining monomer and crosslinker in deionized water to obtain the desired concentration. Immediately prior to each experiment, 20 μL of a freshly prepared 10 % w/v aqueous APS solution was added to 2 mL of the gel stock solution and gently mixed. Hydrogel disks (~180 μL in volume) were polymerized in the parallel plate fixture of a rheometer fitted with a UV curing stage (see description of rheological experiments) in order to allow G' (and hence the average pore size) to be measured during the crosslinking reaction.

The term %T refers to the total mass of monomer and crosslinker per unit volume of gel solution, while %C refers to the mass of crosslinker relative to the combined mass of monomer and crosslinker, as follows[41, 42].

$$\%T = \frac{m_{monomer}(g) + m_{crosslinker}(g)}{V_{solution}(mL)} \times 100 \qquad (2.1)$$

$$\%C = \frac{m_{crosslinker}(g)}{m_{monomer}(g) + m_{crosslinker}(g)} \times 100 \qquad (2.2)$$

All reagents were used as received and gel concentrations were chosen to correspond with those typically used in single-stranded DNA electrophoresis. All samples were freshly prepared prior to each experiment and immediately loaded onto the lower plate of the rheometer fixture.

2.2.2 Rheological experiments

Rheological experiments were performed using a Paar-Physica MCR-300 rheometer (Anton Paar Gmbh, Graz, Austria) equipped with a UV curing cell incorporating a parallel-plate geometry with a 25 mm-diameter upper stainless steel plate and an optically transparent lower base plate. An EXFO Omnicure Series 1000 UV source (EXFO, Vanier, Quebec, Canada) was used to control illumination intensity and exposure time. The maximum output of the UV source was 20 W/cm2. A 0.2 mm gap setting was used to minimize the optical path length and ensure uniform UV penetration trough the sample (~ 180 μL loading volume). The rheometer was equipped with a thermoelectric temperature control system, and a temperature calibration of the lower transparent fixture was performed prior to conducting experiments in order to ensure

accuracy. Samples were allowed to thermally equilibrate for several minutes after loading, and a solvent trap was used to minimize evaporation during the course of each experiment.

Oscillatory frequency sweep and strain amplitude sweep experiments were first performed in range of 0.01 – 100 rad/s and 0.1% – 50 %, respectively in order to establish the extent of the linear viscoelastic regime. Based on these data, all subsequent experiments were performed at a strain amplitude of γ^0 = 1 % and an angular frequency of ω = 1 rad/s. To ensure reproducibility, the UV light was activated 40 s after initiation of the rheometer program. Samples were exposed to UV illumination for a period of 1000 s and data was acquired every 5 s. All runs were repeated at least four times. Experiments yielded values of the storage modulus $G' = (\sigma^0 / \gamma^0)\cos\delta$ and loss modulus $G'' = (\sigma^0 / \gamma^0)\sin\delta$ in terms of the phase difference δ between stress and strain.

2.3 Influence of UV intensity

Evolution of the hydrogel network can be followed by observing corresponding changes in the storage modulus G' as a function of time during polymerization (Figure 2.1). These data suggest that, in general, the polymerization process can be decomposed into three regimes. First, there is a brief incubation period in which the

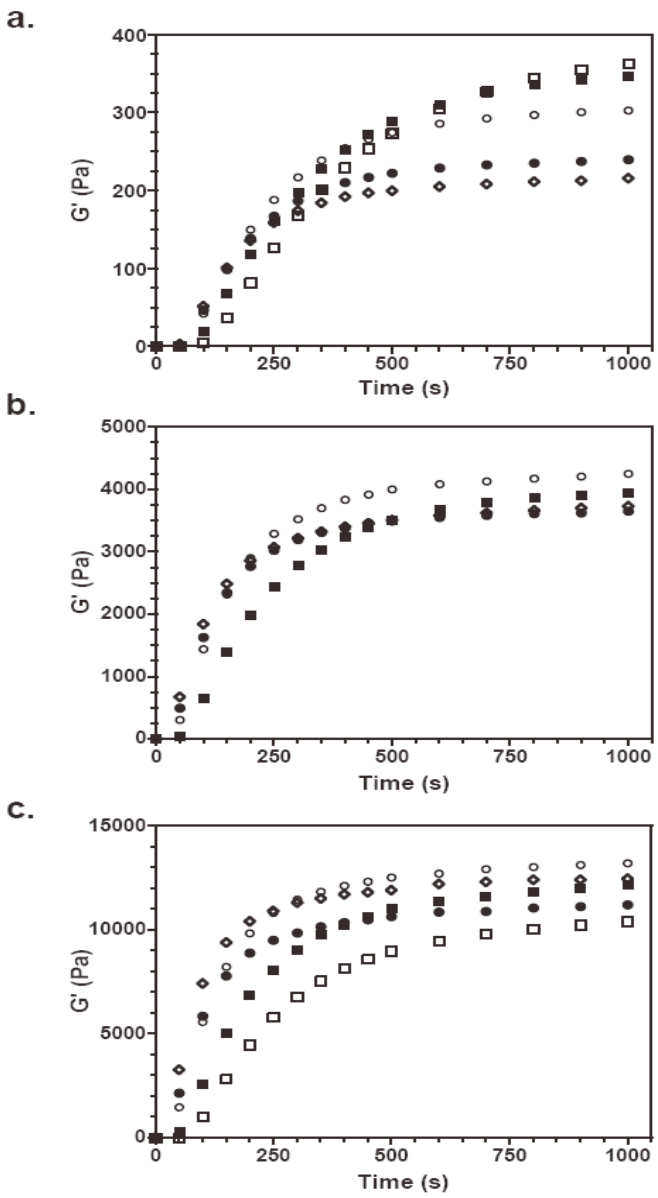

Figure 2.1 Evolution of the storage modulus G' during photopolymerization of LongRanger crosslinked polyacrylamide hydrogels at T = 20 °C. Data are shown for gel compositions of (a) 6, (b) 9, and (c) 12 %T polymerized under UV intensities of [□] 85, [■] 150, [○] 325, [●] 520, and [◇] 735 mW/cm^2.

(a)

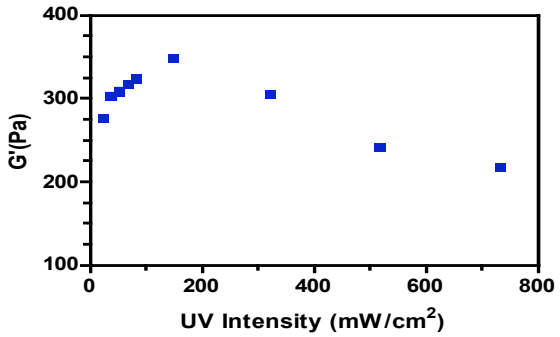

(b)

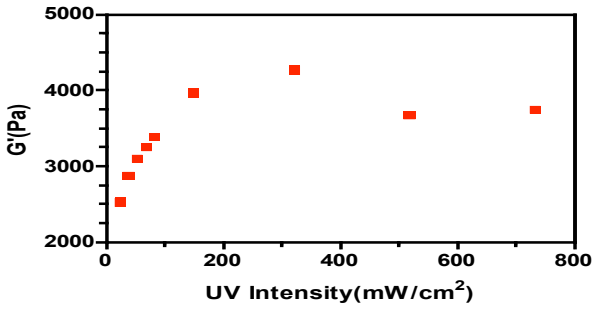

(c)

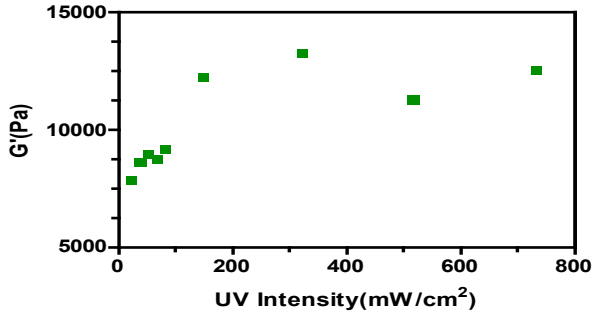

Figure 2.2 Dependence of the steady-state (plateau) value of G' after 1000 s of polymerization on UV intensity. Data are shown for gel compositions of (a) 6, (b) 9, and (c) 12 %T polymerized at T = 20 °C. Note that 25 mW/cm^2 is the lower limit of UV intensity that could be applied using the rheometer's illumination system.

system behaves as a viscous liquid ($G' < G''$) until the gelation point is reached (taken as the point where $\tan \delta = G'' / G' = 1$). After the onset of gelation, G' increases rapidly with time until a plateau is reached in which G' increases more gradually toward an equilibrium value. The magnitude of the loss modulus G'' remains small during the entire polymerization process (typically less than 0.5 % of G' after onset of gelation). In the 9 and 12%T gels, the plateau values of G' (taken to be the value after 1000 s of polymerization) are much larger in magnitude than those in the 6%T sample. For example, G' increases from approximately 200–12,000 Pa as the gel concentration is increased from 6 to 12 %T at 735 mW/cm^2 UV intensity.

The plateau value of G' increases with increasing illumination strength at low UV intensities (i.e., below, 150 mW/cm^2) for all gel concentrations studied (Fig. 2.2). Under stronger illumination conditions, however, the plateau value of G' decreases monotonically with increasing UV intensity in the 6%T gel but remains relatively constant in the 9 and 12 %T gels, even displaying a local maximum in the vicinity of 325 mW/cm^2 In the 6 %T gel, the plateau value of G' (taken to be the value after 1000 s of polymerization) decreases with increasing UV intensity. In the 9 and 12 %T gels, however, the plateau values of G' exhibit a maximum at a UV intensity of 325 mW/cm^2 and are much larger in magnitude than those in the 6 %T sample. The variation of gelation onset as a function of UV intensity is shown in Figure 2.3. In all

cases, the gelation point occurs more rapidly as the UV intensity is increased, as expected due to the increased dissociation rate of the initiator into free radicals. In terms of the elapsed time prior to onset of gelation (t_{onset}), the observed timescales are somewhat longer in the 6 %T sample, with much less of a difference between the 9 and 12 %T gels.

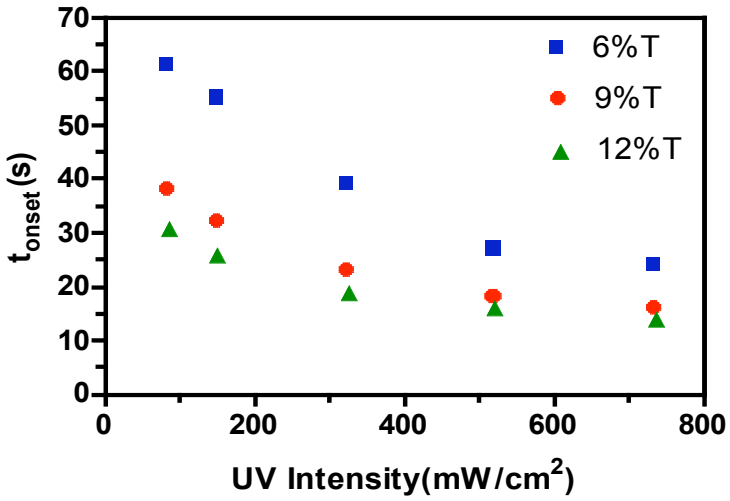

Figure 2.3 Variation of the elapsed time for onset of gelation (t_{onset}) with UV intensity during photopolymerization of LongRanger crosslinked polyacrylamide hydrogels. Data are shown for gel compositions of [■] 6, [○] 9, and [▲] 12 %T polymerized at T = 20 °C.

In the generally accepted picture of microstructural evolution during polymerization, an initial period exists in which spatially distinct, highly crosslinked *microgel clusters* are formed by preferential cyclization of pendant vinyls[13, 15] and crosslinking between monomers not associated with growing chains[43-45].These clusters contain excess crosslinker owing to its higher reactivity relative to acrylamide monomer. As polymerization proceeds, less crosslinker is available for incorporation within individual clusters, resulting in formation of a global gel network via reactions involving remaining active sites on end groups and peripheral pendant vinyls. Consequently, it is postulated that the resulting hydrogel consists of an inhomogeneous assembly of tightly crosslinked microgel clusters interconnected by a more lightly crosslinked network. The pore structure of this interdomain gel network serves as the sieving matrix for DNA electrophoresis.

At intensities below 150 mW/cm^2 UV illumination strength strongly influences the rate of polymerization through its effect on initiator decomposition rate, as reflected in the observed increase in the plateau value of G' with increasing intensity. At intensities above 150 mW/cm^2, the influence of UV illumination on the gel structure appears to be concentration-dependent. In the 6 %T hydrogels, for example, both the crosslinker and acrylamide monomer concentrations are relatively low. Since increased UV intensity promotes initiator decomposition, it is possible that a considerable fraction of

monomer and crosslinker will be consumed during the microgel cluster formation process, leaving less available for interdomain crosslinking. If this is the case, the effect of increasing UV intensity will primarily be to promote increased cyclization within the clusters thereby resulting in the observed reduction in the steady-state value of G'. Thus, although more clusters are generated with increasing UV intensity, there may be fewer elastically active interdomain junctions due to the reduced amount of monomer and crosslinker present during later stages of the reaction. In the 9 and 12 %T hydrogels, overall monomer and crosslinker concentrations are higher, increasing the number of active strands available for crosslinked network formation. At some point, however, polymerization kinetics may become so rapid that diffusive transport of monomer and crosslinker molecules to active sites on growing polymer chains are inhibited by the rapidly forming gel network, resulting in the observed saturation in G' at intensities above 150 mW/cm^2 (Figure 2.2). The apparent local maximum in G' observed at a UV intensity of 325 mW/cm^2 may reflect the influence of cyclization effects, which are likely to become more pronounced at higher UV intensities because of the enhanced initiator decomposition rate.

2.4 Influence of polymerization temperature

In the case of free radical polymerization with chemical initiation, temperature exerts an influence at all stages of the process, with the activation energy associated

with initiator decomposition generally greater than that of either the propagation or termination steps[26, 46, 47]. In the case of photopolymerization, the initiator dissociation rate is expected to depend primarily on UV light intensity rather than temperature. This is evident in the data for the plateau value of G' shown in Figure 2.4a, where an increase with temperature is observed primarily at the lowest UV intensities. The gelation point also exhibits temperature dependence, with onset occurring more quickly at higher temperatures (Figure 2.4b). Nevertheless, UV intensity exerts a much stronger influence than temperature (see Figure 2.2).

2.5 Effect of initial monomer concentration

Although previous studies have investigated the effects of initial monomer concentration on hydrogel properties such as swelling behavior [36], microstructure[39] and homogeneity[34], the relationship between initial monomer concentration and rheological properties has not been widely explored in crosslinked polyacrylamide hydrogels. Classical rubber elasticity theory suggests the following relationship

$$G' = nRT \qquad (2.3)$$

where n is the number density of elastically effective covalent entanglement points (mol/m^3) and the plateau value of the storage modulus G' has been substituted in place of the elastic modulus G (since $G'' << G'$). Thus, at a given reaction temperature T an increase in the number of network junctions is expected to be accompanied by a

(a)

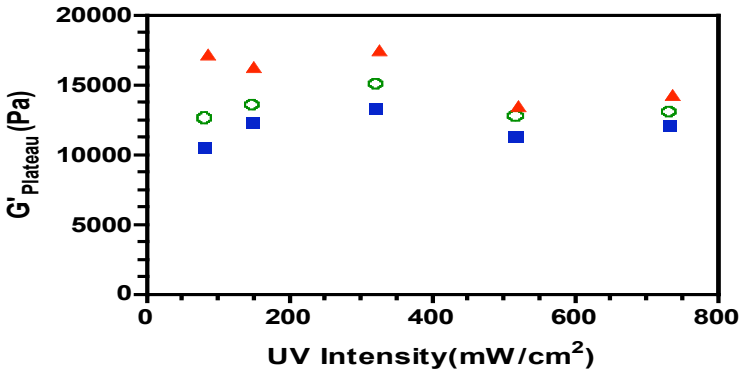

(b)

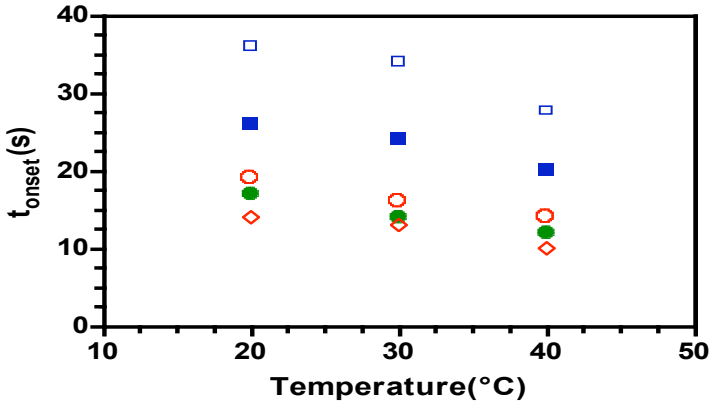

Figure 2.4 Influence of polymerization temperature during photopolymerization of a 12 %T LongRanger crosslinked polyacrylamide hydrogel. (a) Variation of the plateau value of the storage modulus G' with UV intensity during photopolymerization at temperatures of [■] 20, [○] 30, and [▲] 40 °C. (b) Evolution of the gelation onset time t_{onset} with temperature during photopolymerization at UV intensities of [□] 85, [■] 150, [○] 325, [●] 520, and [◇] 735 mW/cm^2.

proportional increase in the steady-state value of the storage modulus. The molecular weight of the polymer chain segments linking two microgel clusters can then be estimated from the number of active junctions n and the total acrylamide monomer concentration $[AAm]$ as follows[48].

$$M = \frac{[AAm]}{n} \qquad (2.4)$$

Our studies of the Long Ranger formulation were motivated by its relevance in DNA electrophoresis applications. This choice presents a trade-off, however, since the Long Ranger gel is supplied as a premixed monomer and cross-linker solution and it is not possible to independently vary the concentration of the individual components. As shown in Figure 2.2, the plateau value of the storage modulus increases by more than a factor of 10 as gel concentration is doubled from 6 to 12 %T. This dependence is in general agreement with the observations of Trompette et. al.[39] in polyacrylamide hydrogels crosslinked with bisacrylamide, where the magnitude of the complex shear modulus $|G^*|$ was found to scale with $[AAm]^{3.3\pm0.2}$. Some deviation from this scaling is to be expected, however, because LongRanger gels employ a slightly different proprietary crosslinker formulation.

2.6 Effect of crosslinker

Although studies using the LongRanger gel formulation were motivated by its applicability as a high-resolution sieving matrix for DNA sequencing, the fact that it is

supplied as a pre-mixed solution did not permit the crosslinker concentration to be varied. In order to investigate the influence of crosslinker concentration, a series of experiments were performed using gels prepared from acrylamide and bisacrylamide powder. Gel compositions of 6 %T with crosslinker concentrations ranging from 1 to 8 % C were selected to be representative of typical formulations relevant to DNA electrophoresis.

The plateau value of the storage modulus G' increases with crosslinker concentration, and the timescale for onset of gelation decreases with crosslinker concentration over the entire range of formulations studied (Figure 2.5). This is expected based on the enhanced capability to form active elastic junctions when additional crosslinker molecules are available for incorporation into growing polymer chains. This effect, however, is also accompanied by a corresponding increase in the number of pendant vinyl groups available for cyclization. The effect on t_{onset} is most pronounced at the lowest values of %C, in agreement with previous results [35].

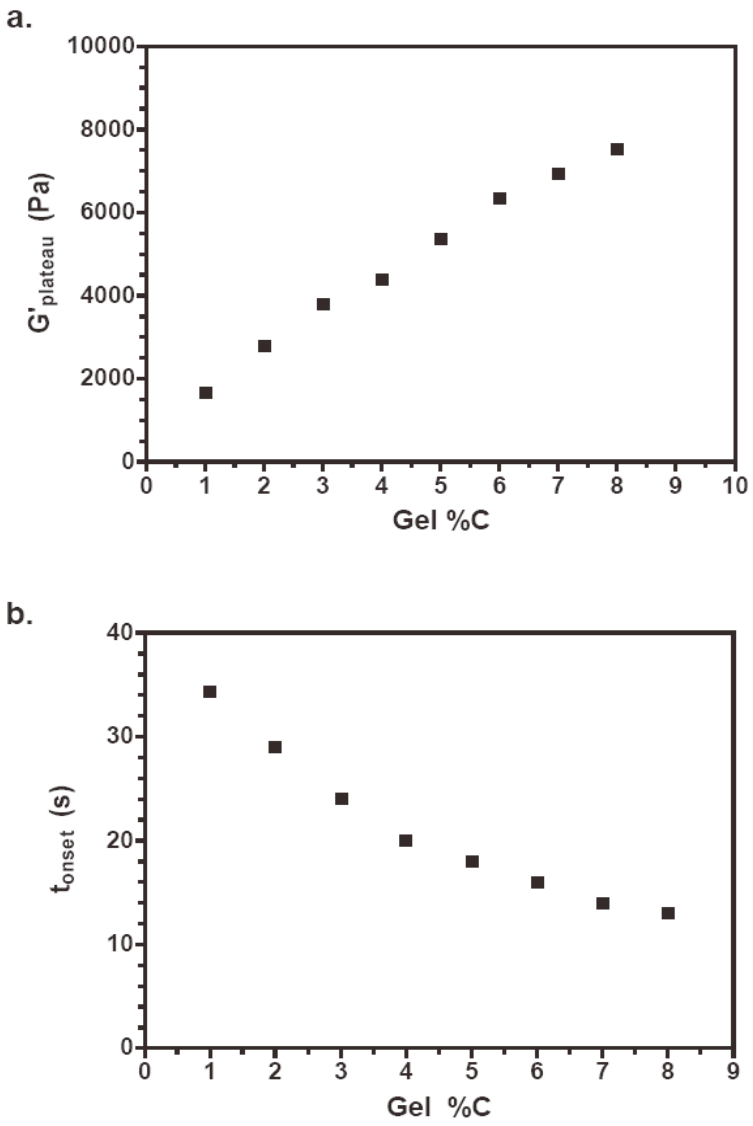

Figure 2.5 Influence of crosslinker concentration in a 6 %T crosslinked polyacrylamide hydrogel. Evolution of (a) the plateau value of the storage modulus G', and (b) the gelation onset time t_{onset} are plotted for crosslinker concentrations ranging from 1 – 8 %C. Polymerization conditions: T = 20 °C, UV intensity = 325 mW/cm^2.

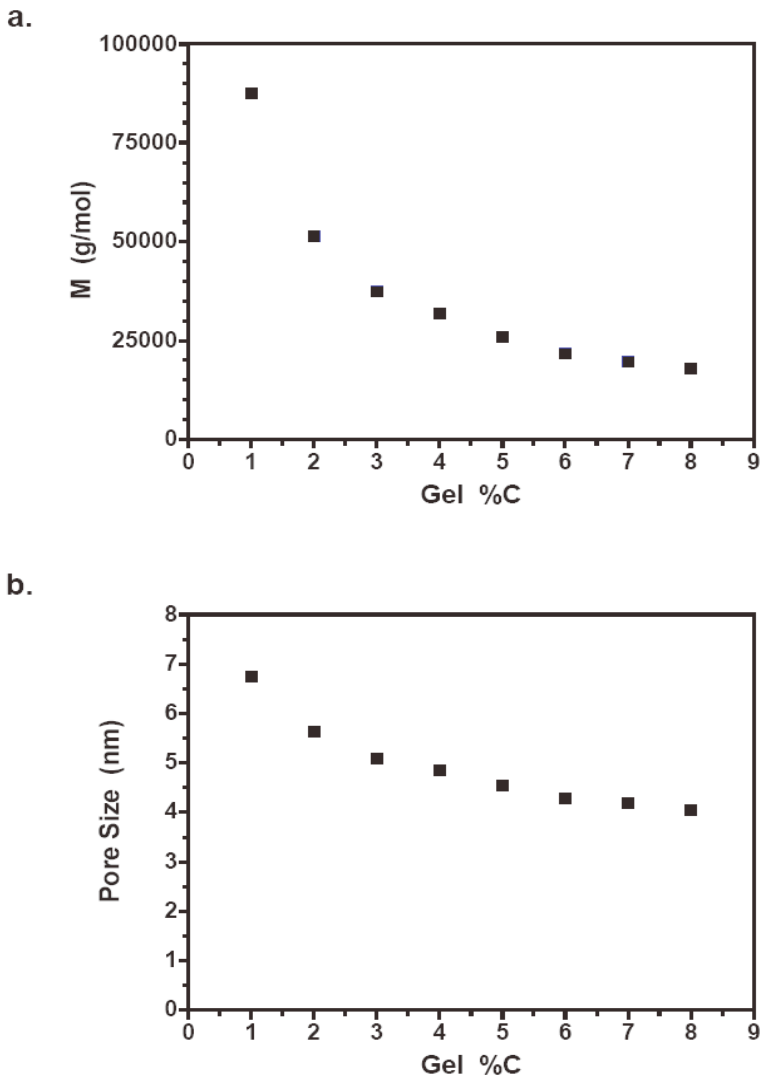

Figure 2.6 Effect of crosslinker concentration on gel pore structure in a 6 %T crosslinked polyacrylamide hydrogel. Evolution of (a) crosslink strand molecular weight, and (b) average pore size ($L/2$) estimated from Equation 5 are plotted for crosslinker concentrations ranging from 1 – 8 %C. Polymerization conditions: T = 20 °C, UV intensity = 325 mW/cm^2.

An estimate of the number of active junctions in the hydrogel network can be obtained using classical rubber elasticity theory (Equation 2.3), which indicates that the increase in the plateau value of G' with %C is accompanied by a corresponding increase in number density of junctions. This increase in junction density is in turn accompanied by a decrease in the average molecular weight of polymer strands linkingtwo neighboring junctions (Figure 2.6 a), suggesting that the gel network is interconnected with shorter crosslinks and incorporates a smaller average pore size.

2.7 Average gel pore size

The electrophoretic migration behavior of DNA fragments in a gel matrix is largely dependent on the relative magnitude of the equilibrium coil size of the migrating DNA molecules to the characteristic gel pore size[49], making the pore size and its distribution one of the most important parameters in selecting an appropriate electrophoresis gel matrix formulation. Hence, it is of interest to develop a straightforward method to estimate average gel porosity from rheological response data. In the case of crosslinked polyacrylamide, DNA transport occurs primarily through the lightly crosslinked regions between microgel clusters. Consequently, an estimate of the matrix pore size can be extracted from the average spacing between entanglement clusters [50]. In this simplified analysis, it is assumed that the junctions (i.e. clusters) are evenly dispersed and that each junction is positioned in the center of a cubic-shaped

volume element. Since all cubic elements combine to span the total gel volume, and since the total number of junctions can be deduced from Equation 2.3, an expression for the length L of a side of the cubic element can be obtained, from which the half length $L/2$ may in turn be taken as a measure of the characteristic gel pore radius.

$$L = \left(\frac{1}{nN_A}\right)^{1/3} = \left(\frac{RT}{G'N_A}\right)^{1/3} \qquad (2.5)$$

Figure 2.6b shows the results of this analysis for a 6 %T hydrogel with increasing crosslinker concentration. At low concentration, the pore size decreases sharply from 7 to 5 nm, then continues to decrease more gradually with increasing %C. These results are in qualitative agreement with those of Tsong-Pin Hsu etc[51] who reported average pore sizes in the vicinity of 9 – 10 nm from electron microscopy of glycerinated 5.1 %T hydrogels, where the lower gel concentration would be expected to yield a more porous network. In electrophoresis literature, gel pore size estimates are often obtained from measurements of size dependent mobility of DNA fragments[52, 53]. The pore size estimates obtained from rheology in this study P_R can thus be compared with corresponding DNA electrophoresis results P_E using identical gel formulations[53, 54] in order to assess the validity of the simplified model employed here. Remarkably good agreement is observed between both methods, with the ratio of P_R/P_E close to unity for all gel compositions studied—a somewhat surprising result considering that such factors as differences in measurement technique, simplicity of the rheological model,

and polydispersity in the gel pore size distribution are not taken into account in this analysis. For example, in the case of the LongRanger gels, application of Equation 5 using rheological data obtained at a polymerization temperature of 20 °C and UV intensity of 325 mW/m^2 yields pore radius values of 12, 4.9, and 3.4 nm in the 6, 9, and 12 %T gels, respectively. These estimates agree remarkably well with data obtained from corresponding gel electrophoresis experiments (Table 2.1a), especially considering that such factors as differences in measurement technique, simplicity of the rheological model, and polydispersity in the gel pore size distribution are not taken into account in this analysis. We explored this further by comparing electrophoresis-based and rheology-based pore size estimates in a series of photopolymerized gel formulations prepared using riboflavin and Irgacure initiators (Table 2.1b). Again, good agreement is observed between the two techniques. These results suggest that rheological data combined with a straightforward analysis based on classical rubber elasticity theory is capable of providing realistic estimates of average pore size in crosslinked polyacrylamide hydrogels.

Table 2.1 Comparison between pore size estimates determined from rheological measurements and estimates determined from electrophoretic mobility measurements of DNA migration in the gel matrix.

(a) Photopolymerized LongRanger gel formulations of varying composition.

Gel composition	Pore radius (nm)		P_R/P_E
	Rheology (Equation 2.5)	Electrophoretic mobility [43]	
6 %T	12	9.6	1.25
9 %T	4.9	5.2	0.94
12 %T	3.4	3.7	0.92

(b) Crosslinked polyacrylamide hydrogels (9 %T, 5 %C) polymerized using varying photoinitiator amounts and compositions. Photoinitiator amounts represent the quantity added to a 2 mL volume of gel stock solution (see Materials and Experimental Methods section for details).

Riboflavin (μL)	Irgacure 651 (μL)	Pore radius (nm)		P_R/P_E
		Rheology (Equation 2.5)	Electrophoretic mobility [45]	
2.5		3.0	2.7	1.11
5.0		3.2	2.8	1.14
10		3.2	2.9	1.10
	3.0	2.9	2.5	1.16

The apparent agreement between pore size estimates derived from electrophoresis experiments and those obtained using Equation 2.5 is surprising and somewhat counterintuitive. In the case of electrophoretic mobility measurements, it would seem reasonable to expect corresponding pore size estimates to be weighted toward larger pores that would be more accessible to the migrating DNA fragments (i.e., yielding an overestimate of the actual pore size). In the case of rheological experiments, on the other hand, interpretation of the data in the framework of rubber elasticity theory implies polymerization proceeds to a level of 100% conversion and ignores cyclization effects (i.e., it is assumed that all crosslinkers are actively associated with interchain junctions). Thus, Equation 2.5 would be expected to underestimate the actual pore size. Based on these arguments, then, it is not immediately clear why our results suggest good agreement between the two techniques. At present we are not able to offer a complete explanation, although it is likely that details associated with the pore size distribution may play a role. It has also been observed that the presence of denaturants can influence cyclization[29]. Nevertheless, these observations point to the need for more detailed quantitative studies of pore structure in crosslinked polyacrylamide hydrogel sieving matrices.

2.8 Rheology of hydrogels synthesized from monomer/ crosslinker

The hydrogels studied in this section are synthesized from a simple formulation

containing only the solution of acrylamide monomer and Bis crosslinker powder with APS as the initiator. In general, the polymerization process is similar to the two hydrogel formulations previously studied and is also composed of three different stages: (1) An initial period, G' and G'' are small but $G''>G'$.The system behaves as a viscous liquid. An increase in G' occurs after onset of the UV illumination until it equals to G'' at the gel point.(2) A further increases in G' in a sol-gel transition period until it later reaches the plateau region achieving a stable equilibrium value. (3) A further increase in G' toward a final equilibrium stage.

The effects of UV intensity, monomer/crosslinker concentration on the G' of hydrogels are shown in Figure 2.7. The plateau values of G' almost increase linearly with increasing UV intensity for all the gel concentrations studied as shown in Figure 2.7a. This can be explained by the enhanced dissociation of the initiator at higher UV intensity thus making the reaction faster and promote formation of more active strands and junctions. The values of the storage modulus G' also increase sharply with higher monomer concentration (Figure 2.7b). This is expected as more active elastic stands will form with increasing monomer concentration and the microgels will be tightly entangled and strongly connected by those strands. This makes the hydrogels more compact and elastic, resulting in an almost linear increase in the values of storage modulus.

(a)

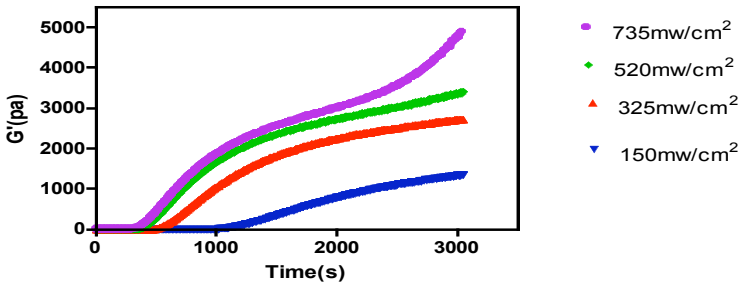

(b)

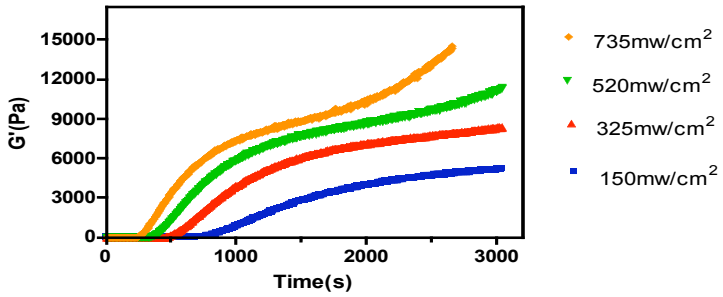

(c)

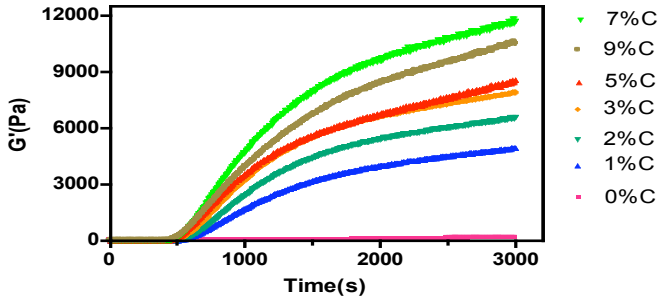

Figure 2.7 Evolution of the storage modulus *G′* during photopolymerization of crosslinked polyacrylamide hydrogels at T = 20 °C. Data are shown for gel composition of (a) 6 %T-5 %Cand (b) 9%T-5 %C polymerized under UV intensity of 735, 520, 325, 150 mW/cm^2. (c) The storage modulus *G′* of 9%T hydrogel as a function of crosslinker concentration under UV Intensity of 325mW/cm^2.

(a)

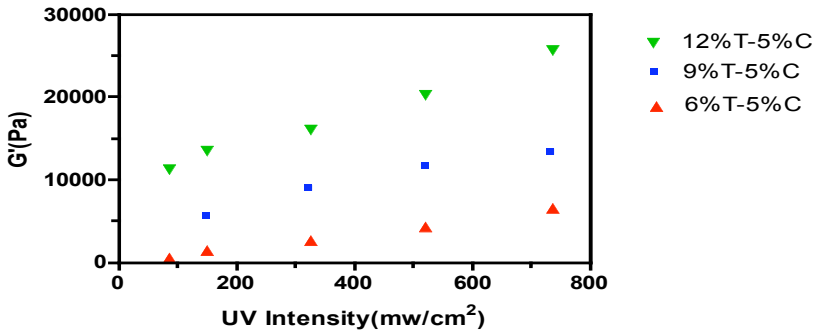

(b)

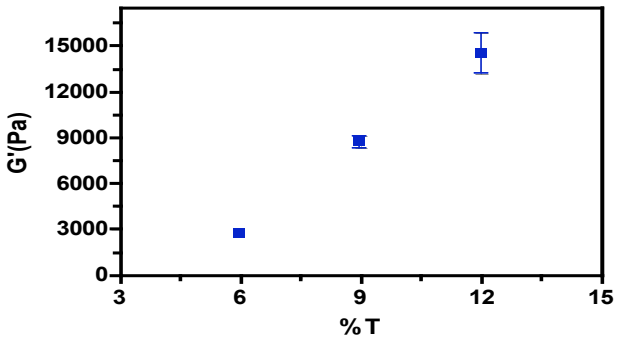

(c)

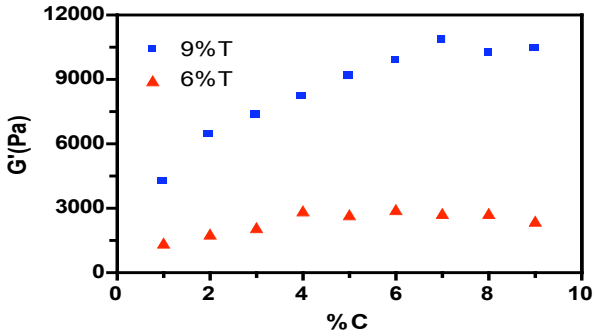

Figure 2.8 Influence of UV intensity, monomer / crosslinker concentration on the steady–state (plateau) *G'* value of polyacrylamide hydrogels. Data are shown for the influence of (a) UV intensity (b) %T (C) %C after 3000 s at T = 20 °C.

At low crosslinker concentration, the storage modulus G' has almost a linear relationship with the crosslinker concentration until G' values reach a plateau region (Figure 2.8c). The storage modulus of 6 %T hydrogel reaches the plateau at 4 %C while 9 %T hydrogel maximized at 7 %C. This could be explained by the increasing number of active elastic junction with higher crosslinker concentration at lower %C and thus higher values of storage modulus. However when further increasing of crosslinker concentration, the crosslinker molecules are less efficient in forming more active junctions and the number of active junctions saturates. Side reactions like cyclization are more active with increasing crosslinker concentration. This could explain the plateau values of storage modulus with higher %C.

2.9 Concluding remarks

Photopolymerized crosslinked polyacrylamide hydrogels are of increasing interest in DNA electrophoresis applications owing to their significantly reduced polymerization times, the ability to manipulate gel morphology by adjusting UV illumination intensity, and the ability to precisely position gel matrices inside microfluidic channel networks. In order to explore the gelation process and its influence on the microstructure of the resulting hydrogel, we have performed a series of in-situ rheological experiments to study the influence of UV intensity, monomer concentration, polymerization temperature, and crosslinker concentration on the steady-state value of the storage modulus G' and the

time for onset of gelation tonset.

In a 6 %T hydrogel, the plateau value of the storage modulus G' decreases with increasing UV intensity, while a maximum in the plateau value is observed at a UV intensity of 325 mW/cm^2 for the 9 and 12 %T samples. The value of t_{onset} decreases with increasing UV intensity in all samples. Temperature also exerts an influence on the plateau modulus and gelation onset, although the effect is not as pronounced as that of UV intensity. Doubling the initial monomer concentration in the reaction mixture from 6 to 12 %T increases the plateau value of G' by over an order of magnitude. The average pore size of the hydrogel network was estimated using a simple model based on classical rubber elasticity theory. Despite its simplicity, this model is capable of yielding pore sizes in agreement with those obtained from analysis of DNA mobility during electrophoresis in identical gels.

The viscoelastic properties of photopolymerized crosslinked polyacrylamide hydrogels with very simple formulations have also been studied with *in-situ* rheological techniques. The evolution of the polymerization process was analyzed and it was found that while G' of polyacrylamide hydrogels increases with increasing monomer concentration and UV intensity, the increase in G' with crosslinker concentration is most pronounced at lower %C and reaches a plateau after 7 %C.

Rheological techniques offer a straightforward method to characterize gel pore

network morphology. In addition to more extensive studies spanning a wider range of gel compositions and refinements in models connecting mechanical response to the pore structure, further theoretical and experimental research in the area of reaction kinetics is also needed in order to better understand the complexities associated with the free radical crosslinking polymerization process.

3. RHEOLOGY AT SOL-GEL POINT

3.1 Introduction

Exploring the nature of a material in the vicinity of the gel point (GP) has received increasing interest because it is likely that gel behavior in this region could provide insights about the phase transition and gel structure formation that may be difficult or impossible obtain with other methods[55, 56]. Rheology has become an important gel point characterization tool because rheological experiments are easy and straightforward to perform, and the data provides a direct link between the material's mechanical properties and its structural features. In rheology experiments, parameter often used to characterize a material's response is the phase difference δ ($\delta = \tan^{-1}\frac{G''}{G'}$) between stress and deformation (strain). During the early stage of polymerization for acrylamide solution, G'' is greater than G' (the system is more liquid like), so $\tan\delta > 1$.The value of $\tan\delta$ decreases as the polymerization process goes on. The point where $\tan\delta = 1$ is often taken to represent the onset of gelation, because under these conditions the material is neither fully solid nor fully liquid (Figure 3.1a). After the polymerization process is complete, G' becomes much greater than G''(the material is more solid like), and $\tan\delta \to 0$.

In addition to the point where $\tan\delta = 1$, the gel point can also be defined as a transition point between infinite shear viscosity and zero equilibrium modulus[55-58]. Its

corresponding rheological criteria of the gel point is when $\tan\delta$ becomes independent of frequency, which means that the G' and G'' curves in a frequency sweep experiment become parallel (Figure 3.1b)[55-59]. The bulk modulus at the gel point can be expressed as follows:

$$G(t) = St^{-n} \qquad (3.1)$$

This can be related to G' and G'' measured in a small amplitude oscillary shear experiment by:

$$G'(\omega) = G''(\omega)/\tan(n\pi/2) = \Gamma(1-n)\cos(n\pi/2)S\omega^n \qquad (3.2)$$

In equation (3.1) S is called the gel stiffness or strength of the gelling network at the gel point and n is the relaxation exponent. Both S and n are characteristic parameters for each incipient gel that are closely related to the nature of specific gelling system[55-58, 60]. The gel strength S has unconventional dimensions that depend on the relaxation component ($Pa \cdot s^n$). The values of S and n can be derived from the small amplitude oscillary shear data as followed:

$$n = \frac{2}{\pi}\tan^{-1}\frac{G''}{G'} \qquad (3.3)$$

$$S = \frac{G'(\omega)}{\omega^n \cos(n\pi/2)\Gamma(1-n)} = \frac{G''(\omega)}{\omega^n \sin(n\pi/2)\Gamma(1-n)} \qquad (3.4)$$

Where $\Gamma(1-n)$ is the gamma function of $1-n$

(a)

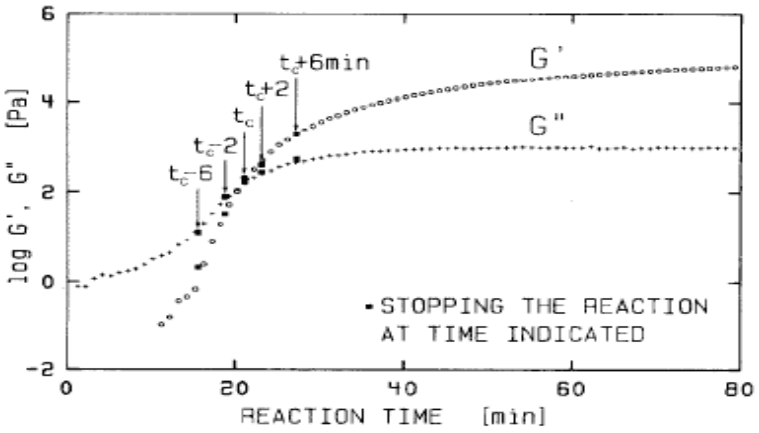

(b)

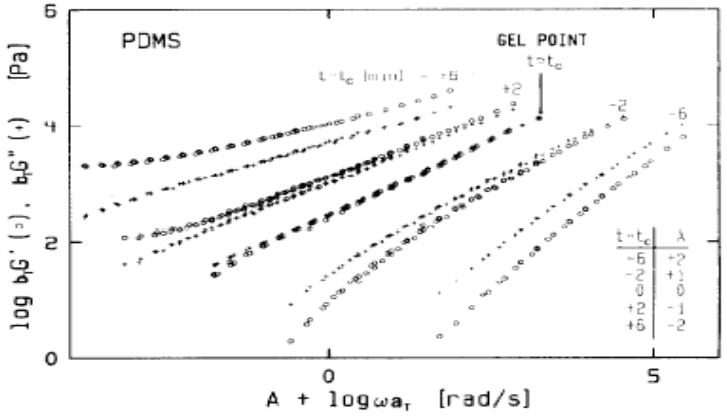

Figure 3.1 Evolution of G' and G'' at gel point. (a) Evolution of the storage modulus G' and the loss modulus G'' of a crosslinking PDMS in an oscillatory shear experiment at constant frequency ω. (b) Reduced storage and loss moduli of PDMS samples for which the reaction has been stopped at intermediate states of conversion. The curves were shifted sideways (factor A) to avoid overlap. Reproduced with permission from the reference 57.

A variety of models have been developed to relate the value of the relaxation exponent n to the gel network structure, such as branching, percolation and fractal theories[55, 61]. The value of n ranges between 0 and 1 and varies with factors including the molecular composition and polymerization conditions. If n approaches 1, the system is more viscous and loose. Whereas values of n approaching 0 indicate that the gelling system is more elastic and compact. Fractal based theories[62, 63] relate the relaxation exponent n with the critical gel structure by representing it in terms of a fractal dimension d_f, defined as $R \propto M^{1/d_f}$, where R is the radius of gyration and M is the molecular weight. Muthukumar[63, 64]suggested that the relationship between n and d_f could be described by equation (3.5) assuming the excluded volume is not screened.

$$n = \frac{d_f}{d_f + 2} \tag{3.5}$$

In the case of full screening of excluded volume, the following equation is used

$$n = \frac{d}{d_f + 2} = \frac{d(d + 2 - 2d_f)}{2(d + 2 - d_f)} \tag{3.6}$$

where $d = 3$ is the space dimension. According to these relationships, values of relaxation exponent between $0 < n < 2/3$ are possible depending on the extent of screening. We follow this picture in the gels studied here as most values of n in our experiments are less than 2/3.

Poly(dimethylsiloxane) (PDMS)[57-59,65], poly(ε-caprolactone) diol (PCL)[66], polyurethanes[65, 67], polycaprolactones[68, 69] and poly (vinyl alcohol) (PVA)[70] systems had been carefully studied with this method and the dependence of n, S and d_f on polymer composition, molecular weight and temperature were investigated. In order to determine the gelation time, multi-frequency sweep experiments are carried out at different time during the gelation process in these experiments. $\tan\delta$ measured with same frequency at different times during polymerization were collected to form a curve and the intercept of these curves was taken as the gel time (Figure 3.2). Most of these systems have a very slow polymerization rate and the reactants are long chain polymers with high viscosity and large G' and G'' at the gel point. So it is safe to assume that relatively little change occurs in the gel network during the continuous frequency sweep experiments.

But this assumption is no longer valid when the reaction rate becomes fast enough that the time for gelation is shorter than the time needed to complete a frequency sweep scan. This limitation is observed when the poly(vinyl alcohol) / poly(acrylic acid) semi-IPN systems (interpenetrating polymer network) was studied with this conventional method[71]. What is more, it is observed that the $\tan\delta$ curves did not crossover at the same time or intercept at two times[72, 73]. Winter[66, 74] noticed this limitation and added toluene solution of elemental sulfur on top of the PDMS sample to stop the reaction near

the gel point. Elemental sulfur even in trace amounts is known to destroy the catalyst for the polymerization of PDMS instantaneously and thus can quench the reaction. However it is difficult to control exactly when to stop the reaction and the quenches might also affect values of measured parameters at gel point. So it is difficult to obtain a material precisely at gel point with this method because of the nature of the transition near gel point.

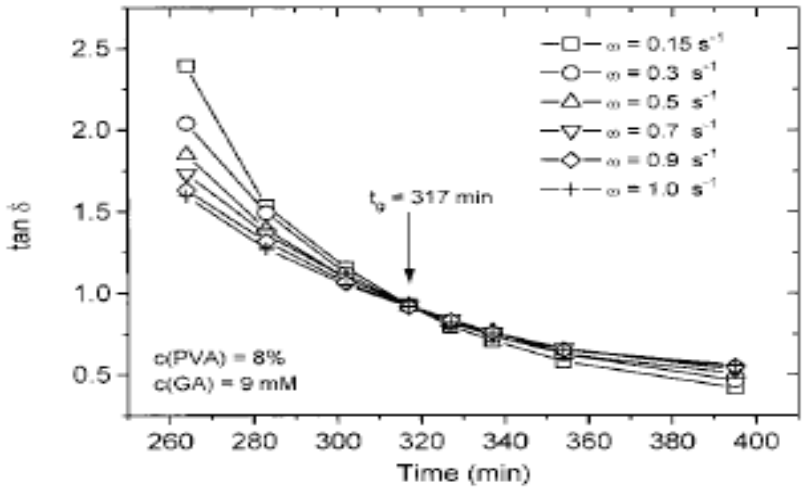

Figure 3.2 tan δ measured simultaneously at different frequencies on a crosslinked poly(vinyl alcohol) system. The notion t_g is the gel time. Reproduced with permission from reference 70.

One of the advantages of photoinititated polymerization is that the gelation process can be stopped immediately when the UV source is turned off, without the need to add other materials to quench the reaction. Critical gel parameters such n, S, d_f can then be derived from the frequency sweep measurement afterwards so that their evolution with monomer / crossliner concentration, UV intensity can be easily studied. Thanks to the photopolymerization technique, a lot of critical gels that could hardly be studied before can now be fully investigated, which will greatly expand the scope of our critical gel systems. At present little is known about the gelation process of photopolymerized system. This study will enhance our understanding of the photopolymerization gelation process and enhance the control of the physiochemical properties of the hydrogels.

3.2 Materials and experimental methods

3.2.1 Materials and hydrogel synthesis

Crosslinked polyacrylamide hydrogels were polymerized from a solution of powdered acrylamide monomer and bis-acrylamide crosslinker with ammonium persulfate (APS) as the initiator. Stock solutions of photopolymerizable gel formulations were prepared by combining monomer and crosslinker in deionized water to obtain the desired concentration. Immediately prior to each experiment, 2 μL of a freshly prepared 1 % w/v aqueous APS solution was added to 2 mL of the gel stock solution and gently mixed. Hydrogel disks (~180 μL in volume) were polymerized in

the parallel plate fixture of a rheometer fitted with a UV curing stage (see description of rheological experiments) in order to allow G' (and hence the average pore size) to be measured during the crosslinking reaction. Following nomenclature used in gel electrophoresis literature [41, 42] (these hydrogels are routinely used as sieving matrix media for electrophoretic separations of DNA and proteins), we express gel concentrations in terms of the monomer concentration ($\%T = \frac{m_{AAM}(g) + m_{CL}(g)}{V_{solution}(mL)} \times 100$) and crosslinker concentration ($\%C = \frac{m_{CL}(g)}{m_{AAM}(g) + m_{CL}(g)} \times 100$), where *AAM* denotes the acrylamide monomer and *CL* denotes the bisacrylamide crosslinker.

All reagents were used as received and gel concentrations were chosen to correspond with those typically used in single-stranded DNA electrophoresis. All samples were freshly prepared prior to each experiment and immediately loaded onto the lower plate of the rheometer fixture to minimize run to run variations.

3.2.2 Rheological experiments at gel point

Rheological experiments were performed using a Parr-Physica MCR300 rheometer (Anton Paar Gmbh, Graz, Austria) with parallel-plate geometry. The diameter of the upper stainless steel plate is 25 mm. The lower plate of the rheometer is transparent glass allowing UV light to pass through from beneath. The rheometer is equipped with a Peltier device that controlled the temperature, and was calibrated before the experiments in order to ensure precise measurements. A solvent trap was used to minimize the

evaporation.

Frequency sweep and strain amplitude sweep experiments were first carried out 0.01~100 rad/s and 0.1%~50% respectively, after which the strain of γ^0=1% and an angular frequency of ω=1 rad/s were chosen to ensure all rheological experiments were performed within the linear viscoelasitic regime and the gel was not damaged or ruptured during the experiments.

An EXFO Omnicure Series 1000 UV source was used that allow the light intensity and exposure time to be set before the experiments. The total output of the UV source is 20 W/cm^2. Samples were exposed to UV illumination for a period of 50 min and data was acquired every 5 s. All runs were repeated at least four times.To find out whether rheometer may influence the gelation system, G' and G'' of the control hydrogels were measured after the UV curing and data were compared with those obtained from in-situ rheology.

3.2.3 Determination of gel point and measurement of S and n

The gel point is taken as a time when $\tan\delta$ is independent of the frequency during the frequency sweep experiments. The UV source is turned off at a specific time and the evolution of the dynamic moduli was measured over a span of three decades of frequency between 0.1 and 100 rad/s. The scans took around 5 minutes. If the curves of $G'$and G'' are parallel and $\tan\delta$ is constant, then the time at which the

UV source was switched off is taken to be the gel point. n and S of the system were calculated according to equation 3.3 and 3.4.

3.3 The rheology of polyacrylamide hydrogels at sol-gel point

The plateau values of storage modulus G' measured during the in-situ rheology experiment could be taken directly as the bulk modulus of the hydrogels. The storage modulus G' could also be obtained with rheology experiments after the UV curing. There is always concern that the rheometer might affect the gelation process and rheological properties of the materials when shearing or pressing the material during the in-situ rheology experiments. We addressed this concern by comparing the rheological data of hydrogels obtained from in-situ and without in-situ rheology experiment. In both methods the UV curing time is the same and the only difference is whether G' was determined by using in-situ rheology during the polymerization process. Our data reveals that there is no detectable difference in any of the hydrogels we have studied in Table 3.1. This implies that any possible influence of the rheometer using in-situ rheology technique is negligible.

Table 3.1 Comparison of rheology data G' (Pa) for polyacrylamide hydrogels obtained from in-situ rheology experiment and after the polymerization process. The data (mean ± s.d) were computed over an ensemble of 5–10 independent samples for each hydrogel.

Hydrogel Content	5 %C			9 %T				
	6 % T	9 %T	12 %T	1%C	3%C	6%C	7%C	9%C
$G'_{in-situ}$	2700±87	8990±304	14500±876	4600±129	7214±314	9940±401	11392±548	10400±189
G'_0	2680±75	8958±512	14709±784	4537±179	7310±565	9859±444	11501±321	10372±558

The photopolymerization process can be controlled by varying the UV intensity, with the reaction stopping completely when the UV light is turned off. This is confirmed by the evolution of G' of 9 %T-5 %C hydrogels as shown in Figure 3.3. The G' value of the system changes little once the UV source was switched off at different times during the polymerization process. This indicates that the photopolymerization reaction rate is essentially dramatically reduced without UV source and it is safe to assume the reaction almost stops during the short frequency sweep scan (~5 min). The gel at critical point could be obtained if we could stop the reaction at the right time.

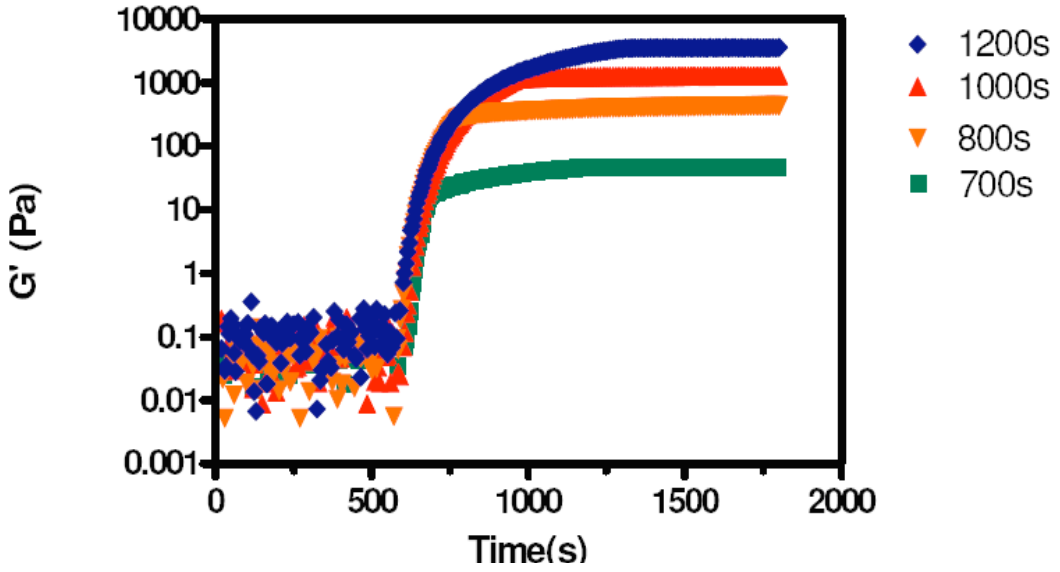

Figure 3.3 The evolution of G' before and after UV light is cut off during polymerization for 9 %T-5 %C polyacrylamide hydrogel. The UV source is switched off at different time (700s, 800s, 1000s, and 1200s) and UV intensity is 325 mW/cm^2.

The polyacrylamide system is a low viscosity liquid with $G''>G'$ during the initial incubation period of polymerization process ($G'$and G''curves of 260 s in Figure 3.4). The frequency dependence curves of G' and G'' are not parallel to each other with G'' curve on the top. As the system approaches the gel point, the two frequency sweep curves become parallel to each other and the values of G" curve are still slightly larger than G' curve ($G'$and G''curves of 266 s in Figure 3.4). This is consistent with the general observation that $G'<G''$ for chemical gels and $G'>G''$

for physical gels at the gel point[56, 75]. After the gel point, G' increases sharply and becomes much larger than G'' (G' and G'' curves of 270s and 275s in Figure 3.4), resulting in formation of a global hydrogel network.

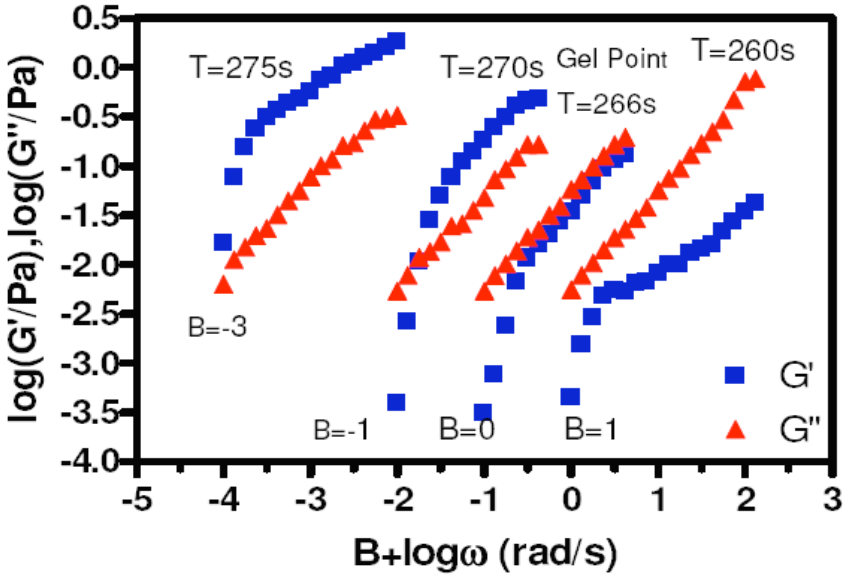

Figure 3.4 G'(■) and G''(▲) of 9%T-5%C polyacrylamide hydrogels polymerized at 520 mW/cm^2 as a function of angular frequency ω at different polymerization time. The data are shifted along horizontal factor B to avoid overlapping.

The gelation time was determined from both $\tan\delta = 1$ (interception of G' and G'' curves) and the time when G' and G'' curves are parallel. The evolution of gelation time with %T%, %C and UV intensity is compared in Figure 3.5. The gel time derived from both methods decreases with increasing UV intensity and monomer

(a)

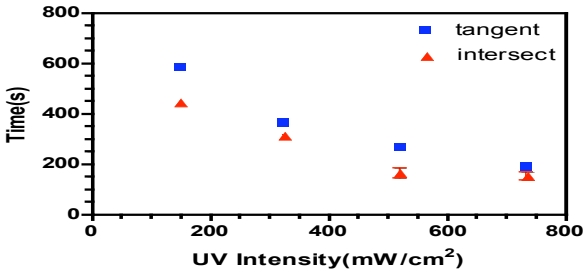

(b)

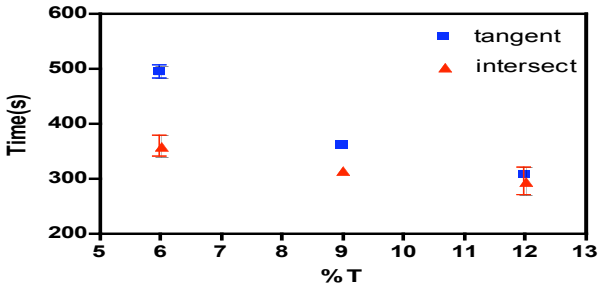

(c)

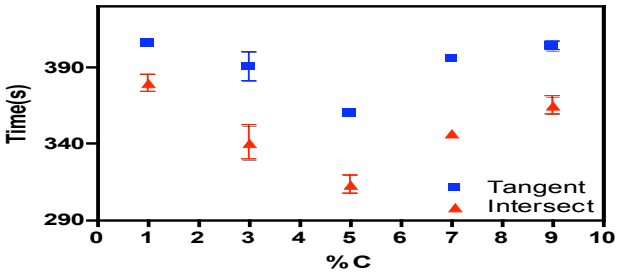

Figure 3.5 Comparison of gelation time derived from two different methods. The gel times are shown as a function of (a) UV intensity for 9% T-5 %C hydrogel (b) %T with 5%C and (C) %C with 9 %T. Blue squares represent the gel time derived from $\tan\delta$ and the red triangle are derived from the crossing point of the G' and G'' curves.

concentration T%. This can be explained that higher UV intensity could promote the dissociation of initiator (APS) into free radicals and thus increases the reaction rate[76], so it takes a shorter time to reach the gelation point. A higher monomer concentration can also promote faster reaction rate in free radical polymerization processes, consistent with our observation that the gelation time decreases sharply with increasing monomer concentration. It is interesting to find that the gelation time decreases with increasing crosslinker concentration from 1 %C, reaches a minimum at 5 %C, and increases again as the crosslinker concentration further increases from 5 % to 9 %C. This is a bit counterintuitive and can be explained that 9 %T, 5 %C may be the optimal combination of monomer and crosslinker concentration. In general increasing crosslinker concentration will enhance the reaction and reduce the gelation time[40, 76]. However, the microgel concentration would also reach a saturation point beyond which fewer new microgels may form when further increasing the crosslinker concentration. Side reactions like self cyclization would also be more likely to occur and consume free radicals with increasing crosslinker concentration, further slowing down the polymerization process and making the gelation time longer.

For the photoinitiated polyacrylamide system, the gelation time obtained from both methods show the same evolution trend regardless of the monomer/crosslinker concentration and UV intensity. The gelation time obtained from the intersection method is 10%~20% shorter than that from the parallel curves method which means that at the intersection point, the real gelation process has not yet started according to the parallel G' and G'' curves method.

The evolution of relaxation exponent n and the gel strength parameter S with T%, % C and UV intensity are shown in Figure 3.6. It is evident that relaxation exponent n decreases while the gel strength parameter S increases with increasing UV intensity. This is expected as higher UV intensity causes faster dissociation of initiator and enhances the formation of more microgels and strands to connect them. This will make the gel at critical point more elastic and stable and result in smaller n and larger S.

The values of exponent n decrease monotonically with increasing monomer concentration %T and the values of corresponding gel strength S increase with monomer concentration at the same time. More elastic strands will form to interconnect the microgels with increasing monomer concentration, which will make the network stronger and more elastic and thus can decrease the slope of frequency sweep curve n and result in larger gel strength S. The values of n decrease with

increasing crosslinker concentration under the same monomer concentration (9 %T), However the decrease rate in the values of *n* is not so sharp after 5 %C. which supports our assumption of the change in the reaction kinetics after 5 %C as described in discussion of the gel time. The values of S shared an opposite trend and increased with higher crosslinker concentration. This could also be explained by growing side reactions with increasing crosslinker concentration.

The fractal dimension was also calculated from equation (3.6) according to the model of Muthukumar [62, 63]. The effects of monomer and crosslinker concentration and UV intensity on the fractal dimension are compared and depicted in Figure 3.6 (b, d, f). The results show that the fractal dimension increases with increasing monomer and crosskinker concentration and UV intensity. This can be explained as more elastically active strands and microgels will be generated with increasing %T, %C and UV intensity, thus making the critical gel network more densely connected and more elastic. These findings are consistent with the generally accepted picture that gels with large factual dimensions possess a more compact structure at the gel point[66, 68, 69, 75, 77].

All the available data of n and S are collected and the plot of S as a function of n is shown in Figure 3.7. The plot indicates that S and n are strongly coupled and might have an approximately linear relationship between them. This result is consistent with the previous observations [66, 68, 75, 78].

(a)

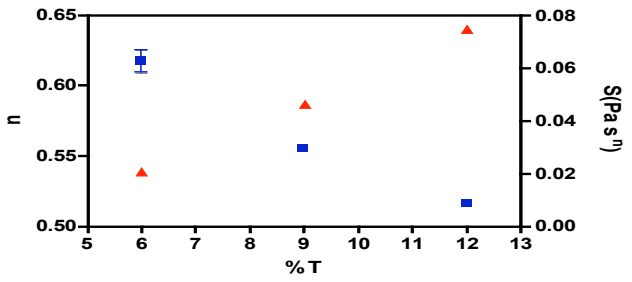

(b)

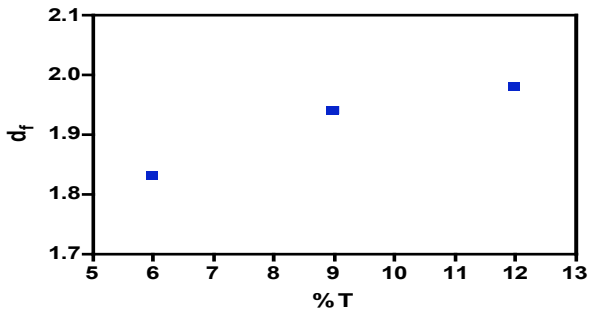

(c)

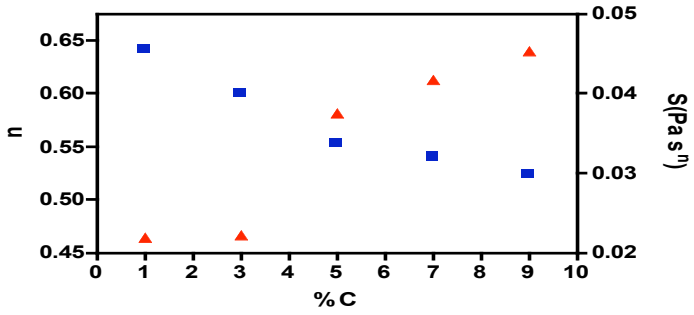

Figure 3.6 The evolution of n, S and d_f with monomer/crosslinker concentration and UV intensity. The values of n, S as a function of monomer/crosslinker concentration and UV intensity are shown in (a) for 5 %C hydrogel, (c) for 9%T hydrogel, (e) for 9 %T-5 %C hydrogel. Evolution of d_f are shown in (b), (d), (f). The UV intensity for Figure 3.6 a-d is 325 mW/cm^2.

(d)

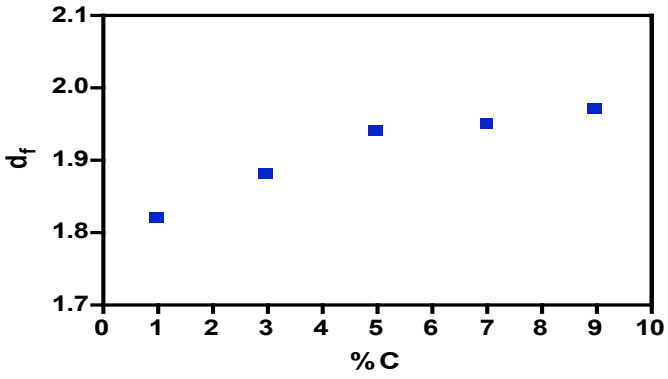

(e)

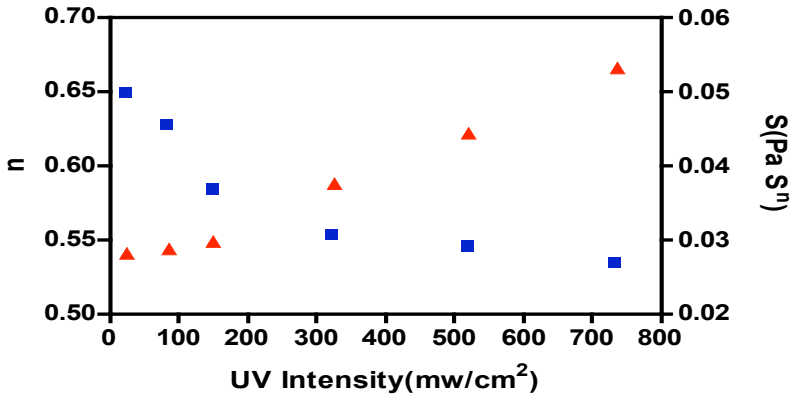

(f)

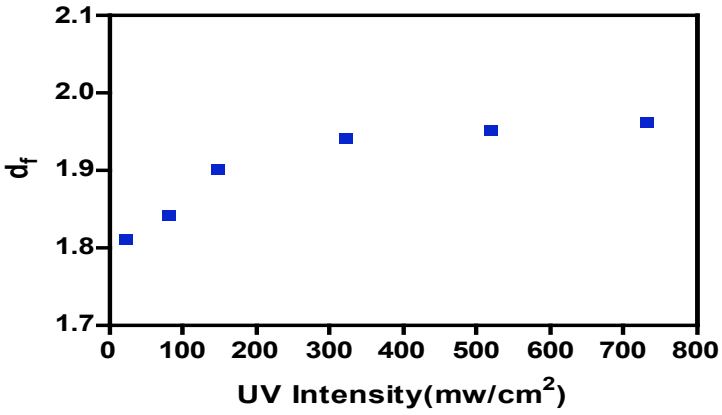

Figure 3.6 Continued

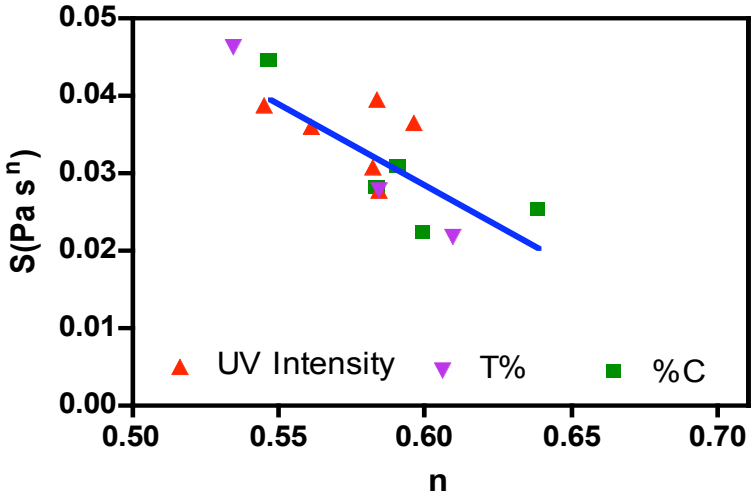

Figure 3.7 Gel strength S as a function of the relaxation exponent n for different hydrogels. Hydrogels used in this figure are [■] 9%T, different %C (1 %, 3 %,5 %,7 %,9 %) hydrogels at 325 mW/cm^2; [▲] 9 %T,5 %C hydrogels polymerized at 150, 325, 520, and 735 mW/cm^2; [▼] (6 %T, 9 %T, 12 %T) hydrogels with 5 %C.

A simple equation (equation 3.7) derived by Winter[78] is used to further investigate the relationship between gel strength S and relaxation exponent n. The gel strength S can be expressed as a combination of the material's characteristic modulus G_0 and relaxation time λ_0 as can be seen in the following equation.

$$S = G_0 \lambda_0^n \qquad (3.7)$$

A least-squares fit of the strength and relaxation exponent data yields that G_0 = 2.1 Pa and $\lambda_0 = 8.6\times10^{-4}$ s, $G_0\lambda_0 = 1.8\times10^{-3}$. The values of S are restricted with $G_0\lambda_0 < S < G_0$. According to Winter's theory[78], the upper limit values of G_0 should be close to the plateau modulus of the polymer. However, G_0 is 2.1 Pa for photopolymerized polyacrylamide hydrogels and is about 1,000 times smaller than the storage modulus G' of fully cured hydrogels (between 2,000~20,000 Pa). This could be explained by the low modulus and viscosity of the system near the gel point and unique characteristics of the hydrogel system.

Most of the n values we measured are located in the approximate range of 0.5-0.7. This feature is consistent with the fact that polyacrylamide hydrogels are relatively fragile and soft, and also matches the value derived from percolation theory (n=2/3)[55, 56].

The evolution of n, S and d_f also reveals their connection with the nanoporous morphology of the crosslinked polyacrylamide hydrogels. The pores of hydrogels are formed due to the inhomogeneity of the network and the pore sizes are supposed to be the average spacing between entangled clusters or microgels[76]. The pore size and pore size distribution of the corresponding cured hydrogels were measured with DSC. These data appear to show that the values of n almost have an almost linear relationship with both the pore size and the pore size distribution of the

fully cured hydrogels. The pore size increases and pore size distribution become wider with increasing n and decreasing S as shown in Figure 3.8 and Figure 3.9. Hydrogels polymerized at low monomer/ crosslinker concentration and UV intensity are generally expected to yield a more porous and softer network and would therefore possess a larger value of n and small S. With increasing monomer/crosslinker concentration and UV intensity, more clusters and active elastic strands will be produced, making the distance between clusters shorter and thus the pore size of hydrogels will be smaller. The hydrogels become more rigid and stiff which means larger S at the same time, therefore possessing smaller values of n. The pore size distribution also narrows as there is less probability of forming very large pores as the gel network grows more compact. These results suggest that n of critical gel could also be an indicator of the pore size of the fully cured hydrogels.

Another interesting finding is that we observed a linear relationship between the values of S and the corresponding plateau storage modulus G' (Figure 3.10). In addition, we find that the slope of a log-log plot of G' vs S is 5.37 ± 0.07 and remains nearly constant regardless of the gel concentration or UV intensity. This finding implies that the critical gel strength S is closely connected with the cured storage modulus of the hydrogels and can serve as an important parameter to indicate the viscoelastic properties of the fully cured gel networks despite their large difference

(a)

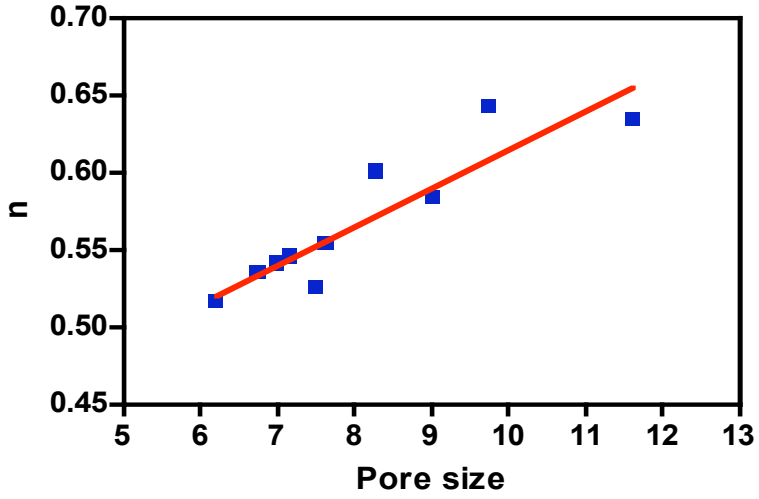

(b)

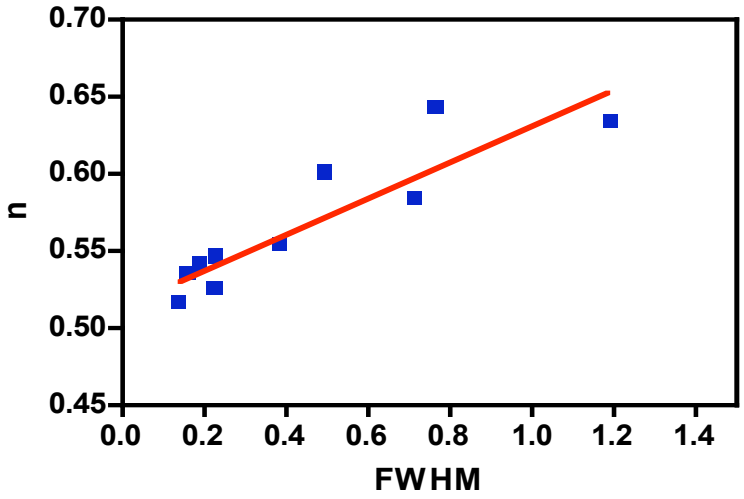

Figure 3.8 The evolution of n as a function of pore size and FWHM. The data are shown for (a) pore size (b) FWHM. All the hydrogels used are the same as shown in Figure 3.7.

(a)

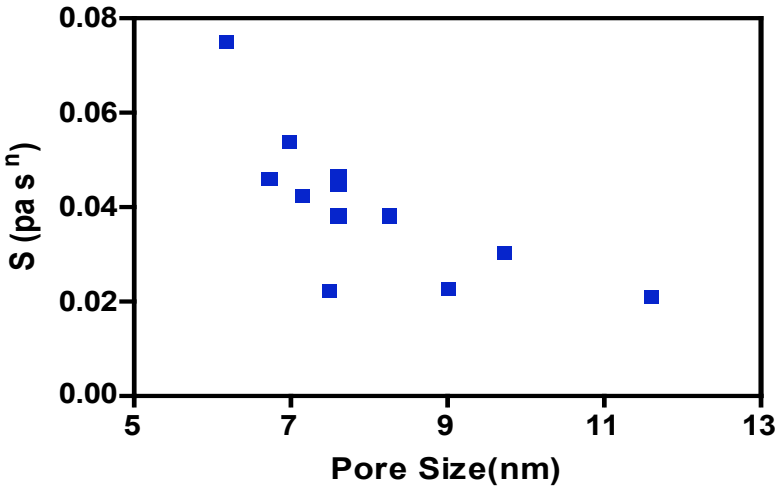

(b)

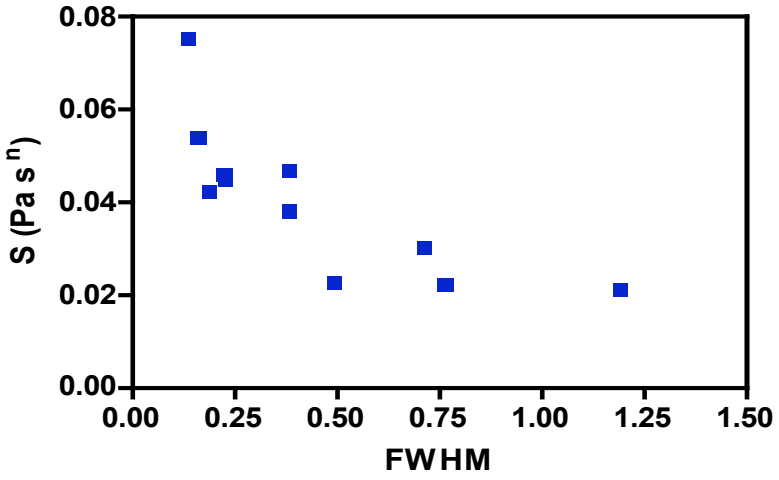

Figure 3.9 The evolution of S as a function of pore size and FWHM. The data are shown for (a) pore size (b) FWHM. All the hydrogels used are the same as shown in Figure 3.7.

in absolute values.

It is not clear to what extent can this linear relationship could be applied to other systems as very little data available for both the critical gels and the fully cured gels. Nevertheless, this observation points to a need for a more detailed investigation of the gels at different states and implies the intrinsic connection among them.

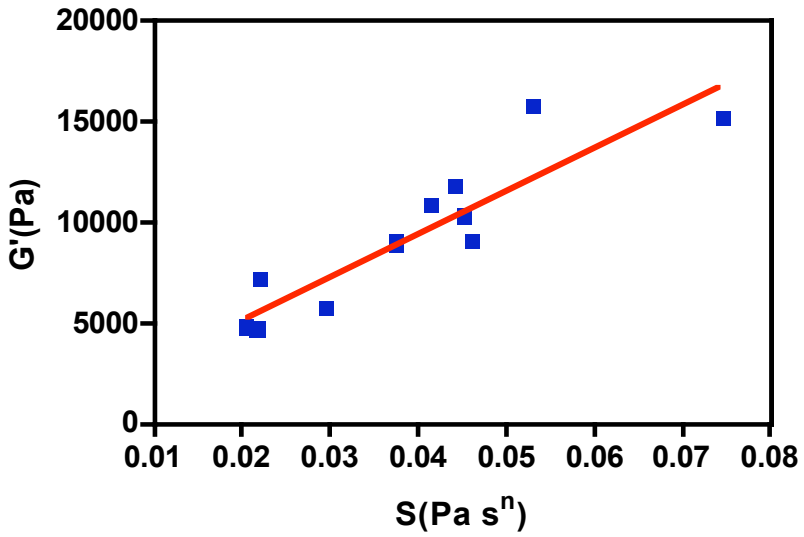

Figure 3.10 Dependence of the storage modulus G' of all cured hydrogels on their corresponding gel strength S. All the hydrogels used are the same as shown in Figure 3.7.

3.4 Conclusion

There is a lack of studies on photopolymerization processes at gel point. We addressed this issue by employing the polyacrylamide hydrogel system whose gel

point rheological properties had not been studied before. The fast reaction rate, small molecule monomer/crosslinker chemistry and low viscosity and modulus at the gel point all hamper the investigation of the system. Photopolymerization chemistry helps to reduce these difficulties because the reaction can be stopped almost immediately when the UV source is turned off. This provides a way to reliably produce critical gel samples whose nanostructure is frozen exactly at the gel point without the need of poisoning the reaction or controlling the stiochiometry reaction. With the help of photopolymerization, many hydrogel systems that could not be studied with conventional methods could be studied now. This will provide new data that can help enhance our understanding of the gelation process in these systems.

There are two different methods to define the gel point and the respective gel time: the $\tan\delta$ method and the interception of G' and G'' curves during in-situ rheology experiment. Data obtained from both methods were compared and appeared to share the same trend though the absolute values were different. For the polyacrylamide system, the gelation time determined using $\tan\delta$ was larger.

The relaxation exponent n and gel stiffness S are intrinsic properties of hydorgels and both values are obtained at the gel point. The relaxation exponent n decreases with increasing monomer/cosslinker concentration and UV intensity while the corresponding values of gel strength parameter S and the fractal dimension d_f

increase under the same conditions. Theses findings suggest the network of the critical hydrogels is strengthened and becomes more tight and elastic with increasing monomer/crosslinker concentration and UV intensity. The modulus G_0 of the polyacrylamide system is much smaller than the plateau values of storage modulus G', in contrast to what has been seen in previous studies of other gelling systems. We find the relaxation exponent n is connected with the pore size and polydispersity of the material. There exists a linear relationship between the critical gel strength parameter S and the storage modulus of the fully cured hydrogels at all the concentrations and UV intensities studied. This suggests a key connection between the critical gel and the fully polymerized network and shows the importance of further studies in the critical gel regime.

4. NANOPOROUS MORPHOLOGY OF PHOTOPOLYMERIZED CROSSLINKED POLYACRYLAMIDE HYDROGELS

4.1 Introduction

A host of characterization methods have been developed to probe the morphological features of porous materials. Some of the techniques can be applied to hydrogels while others can not (Table 4.1). Equilibrium swelling experiments are widely used because the observable quantity is the volumetric ratio between the swollen gel network and its equilibrium (un-swollen) state, which is easily measured by weighing hydrogel samples under both conditions[16, 37, 79-81]. The measured degree of swelling is then related to the average molecular weight between crosslinks, from which a length scale corresponding to an average pore size (or "mesh size") can be extracted.

Peppas and Merrill[16, 80, 81] developed equation 4.1 to estimate the average molecular weight $\overline{M_c}$ between crosslinks. The equation is based on the lattice model theory of Flory and Rehner[82] describing swollen networks formed by crosslinking of a solid polymer. The theory is further extended to consider crosslinking in solution and thus can determine the pore size.

$$\frac{1}{M_c} = \frac{2}{M_n} - \frac{(\bar{\upsilon}/V_1)[In(1-\upsilon_{2,s}) + \upsilon_{2,s} + \chi_1\upsilon_{2,s}^2]}{\upsilon_{2,r}[(\frac{\upsilon_{2,s}}{\upsilon_{2,\gamma}})^{1/3} - \frac{1}{2}(\frac{\upsilon_{2,s}}{\upsilon_{2,\gamma}})]} \qquad (4.1)$$

Table 4.1 Summary of pore size measurement techniques.

Method	Sample prep	Reference	Advantage	Disadvantage
swelling	Easy	16,37,80-83	No damage to hydrogel pores	Many parameters difficult to decide, not suitable for all systems
NMR	Easy	88	No damage to hydrogel pores	Defects in theory and difficult to analyze the results
SANS/SAXS/ Light Scattering	Easy	64,75,86, 87	Not much damage to hydrogel pores	Special equipment/May change the morphology
DSC	Easy	95-101	No damage to hydrogel pores	Only controlled pore glass and membranes well studied
TEM	Difficult (cryo)	51,92,93	Direct visulization and high resolution	No clear pictures have been shown. New preparation methods needed
SEM	Difficult (cryo)	89,92	Direct visulization	Low resolution and pores may be damaged
Rheology	easy	37-40,76	Fast easy	Not direct measurement and can not get the distribution
Mercury Intrusion Porosimetry	Difficult (cryo)	89,92	Suitable for hydrogel with large pores	Difficult to prepare the samples, the hydrogel pores damaged

where M_n is the molecular weight of the uncrosslinked polymer and $\bar{v}$ is the specific volume of the polymer. V_1 is the molar volume of the swelling media and is 18 cm^3/ mol for water. χ_1 is the Flory polymer solvent interaction parameter. $\upsilon_{2,r}$ is the polymer volume fraction before swelling, and $\upsilon_{2,s}$ is the polymer volume fraction of fully swollen hydrogel.

$$\upsilon_{2,r} = \frac{V_d}{V_r} \tag{4.2}$$

$$\upsilon_{2,s} = \frac{V_d}{V_s} \tag{4.3}$$

The mole of the repeat units between two crosslinks n is

$$n = \frac{2\overline{M}_c}{M_r} \tag{4.4}$$

Where M_r is the average molecular weight of the repeat unit. The root mean square end to end distance of the polymer chain could be taken as the approximate pore size of the polymer.

$$(\overline{r^2}) = \ell\sqrt{n} \tag{4.5}$$

Where ℓ is the carbon-carbon bond length and the value is 1.54Å for carbon-carbon bond. The root mean square end to end distance of the polymer chain in the unperturbed state was determined as:

$$(\overline{r_0^2}) = \sqrt{C_n}(\overline{r^2})^{1/2} \tag{4.6}$$

Where C_n is the Flory characteristic ratio of the polymer and the value varies according to different polymer. The pore size (or "mesh size") of the polymer ξ as shown in Figure (4.1) is calculated as

$$\xi = \upsilon_{2,s}^{-1/3}(\overline{r_0^2})^{1/2} \tag{4.7}$$

Parameters like χ_1 and ξ must be known while using this equation however their values are generally difficult to obtain.

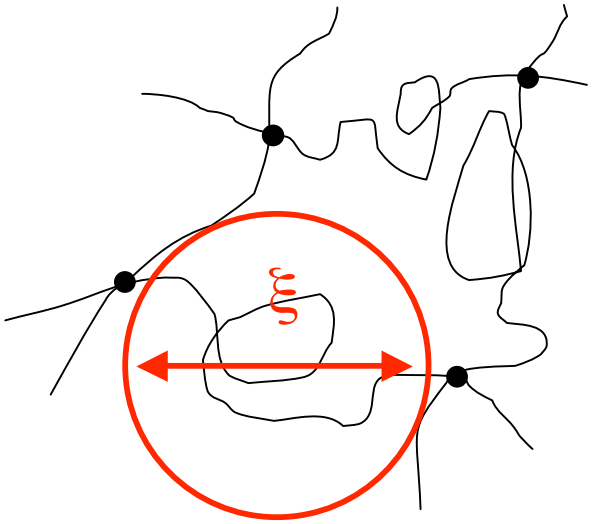

Figure 4.1 The structure of crosslinked hydrogels. The relationship between the pore size of the polymer ξ and the distance of two crosslinks is shown.

Anseth[37, 83] derived another equation based on the rubber elasticity theory to estimate $\overline{M_c}$ from measurements of the compressive modulus. In this model rubber elasticity theory is used to obtain a relationship in terms of a bulk modulus K related to the fractional change in volume of a sample measured in response to uniaxial compression

$$\frac{1}{M_c} = \frac{2}{M_n} + \frac{3K(1-2\nu)}{2(1+\nu)\rho RT(\upsilon_{2,s})^{1/3}} \qquad (4.8)$$

The compressive modulus K could be measured with a dynamic mechanical analyzer (DMA). ρ is the density of the polymer and ν is the Poisson's ratio .

Both swelling models have been developed from an underlying physical picture based on formation of chemical crosslinks between high molecular weight polymer chains (i.e., macromers). Consequently, it is not entirely clear to what extent this framework faithfully represents the morphology of hydrogels like polyacrylamide that are synthesized by free radical copolymerization between monomers and multifunctional crosslinkers. Some physical material parameters of the hydrogels are often needed to obtain the average pore size. For example, the solvent interaction parameter χ_1 must be known to apply swelling-based methods[16, 79], Poisson's ratio ν must be known in compression measurement-based methods[84, 85]. However theses parameters are often difficult to determine.

Scattering (x-ray[64, 86], neutron[75], light[87]) and spectroscopic (NMR[88]) techniques allow gels to be studied in their native hydrated states without being subjected to mechanical contact forces provided that an appropriate structural model can be postulated to interpret the data. But a specialized infrastructure is often needed (e.g., synchrotron facilities, neutron sources) that can render these techniques impractical for routine use.

Nishio[87] studied the pore size of the polyacrylamide by studying polystyrene latex spheres with quasielastic light scattering. The pore size of the polymer could be determined by the following equation:

$$f_{mov}\left[\frac{1}{K}\right] \propto \int_{1/K}^{r_{\max}} V(r)dr \propto I_{mov} / \left\langle I(t) \right\rangle_t \qquad (4.9)$$

f_{mov} is the fraction of the particles that can move through the polymer channels. K is the scattering factor whose magnitude is $|K| = 4\pi \sin(\theta/2)/\lambda$, where n is the refractive index of the solution, λ the wavelength of the laser light, and θ the scattering angel. $r_{\max}$ is the maximum pore size of the material. $V(r)$ is defined as the volume fraction of pores with the size of $r = 1/K + D$ (D is the probe's diameter). $V(r)$ could be derived from equation (4.9) by the derivation of $df/d(1/K)$ as follows:

$$df/d(1/K) \rightarrow V(r) \rightarrow r = 1/K + D \qquad (4.10)$$

The $df/d(1/K)$ curves were measured with samples crosslinked with 500Å probing particles and 1000 Å probing particles (Figure 4.2). The pore size distribution is peaked for the 500 Å data and the most characteristic pore size could be derived from equation 4.10. The average pore size of polyacrylamide hydrogel derived is about 160nm and most of the pores are within the range of 130 nm~210 nm in the experiments. There also exists a lot of small pores in the hydrogel. The structure of polyacrylamide hydrogels were depicted as a large space interconnected by small pores (known as bimodal theory). However the latex spheres in the polyacrylamide solution could influence the reaction kinetics during the polymerization process and it is not entirely clear to what extent the latex spheres could change morphology (pore size) of

the hydrogels. Also it is possible that the pore diameter in hydrogels are smaller than the size of the latex spheres for scattering (50 nm and 100 nm) and the scattering results could not show the entire picture of pore size distribution in hydrogels.

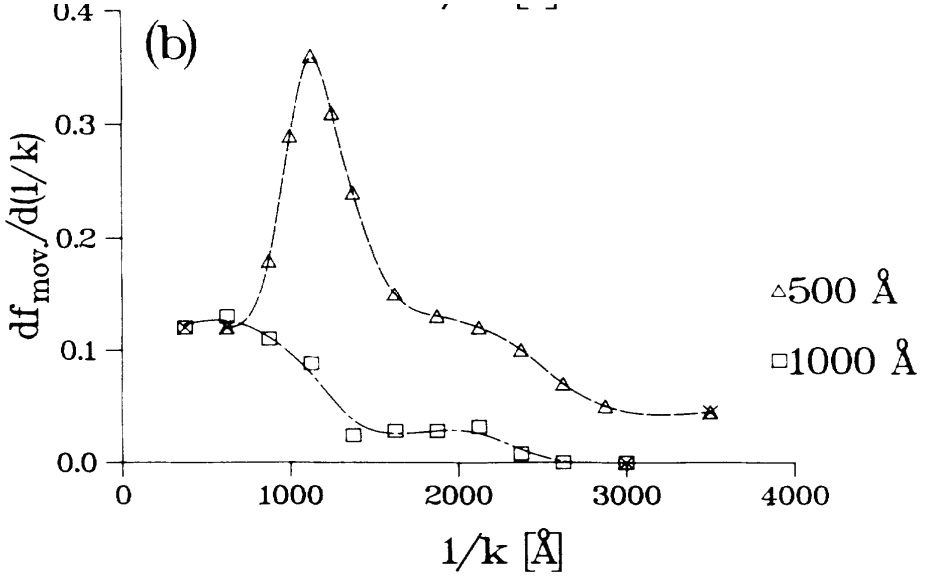

Figure 4.2 Magnitude of the derivative $df/d(1/K)$ for hydrogel samples with different particle size: 500 Å (triangles) and 1000 Å (squares). $f_{BIS} = 1.8\%$ in all samples. Reproduced with permission from reference 87.

McCarthy[88] etc studied the pore size and distribution of the polyacrylamide hydrogels with NMR by measuring the spin lattice relaxation time (T_1).The principle is that the relaxation rate of proton spins in the pores is faster than that in the bulk water because of the stronger interaction between the water and the polymer in the pores.

The simplified working equation is

$$\frac{1}{T_1} = \frac{1}{T_B} + \frac{\psi}{R_h} \qquad (4.11)$$

Where T_1 is the overall spin-lattice relaxation time,which is a weight mean of the bulk relaxation time and the surface relaxation time. T_B is the bulk relaxation time and ψ is the surface sink parameter. R_h is the radius of the pores. The pore size and distribution can be derived from equation 4.11 are shown in Figure 4.3. However there is still discrepancy in the linear relationship between $1/T_1$ and 1/Rh in Equation 4.11 and how to interpret the data. The experiments are difficult to perform and the data is difficult to explain.

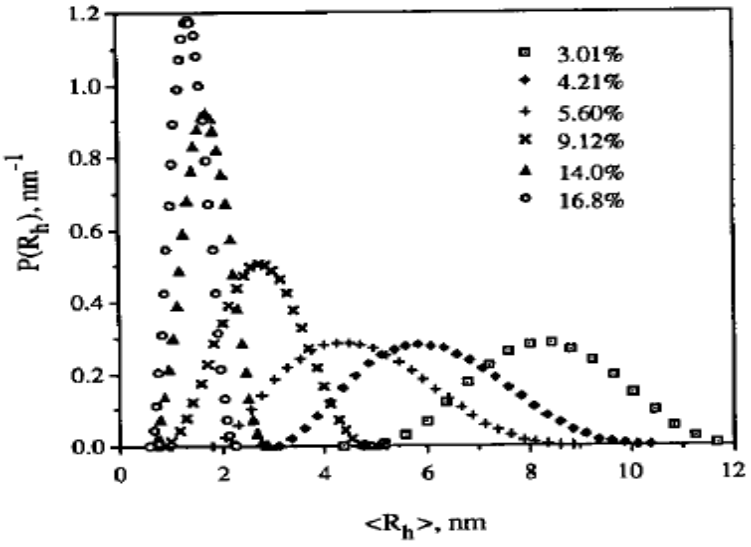

Figure 4.3 Pore radius distribution of polyacrylamide gels by NMR. Reproduced with permission from reference 88.

Intrusion methods (e.g., based on adsorption of nitrogen or mercury[89]) are another class of techniques that are widely used to characterize porous materials, however they cannot generally be applied to study gels in the hydrated state. Instead, water must first be removed by subjecting samples to preparation steps like freeze drying that can damage or destroy mechanically fragile hydrogel networks. This introduces uncertainty about whether the data truly reflect the gel pore structure or have been distorted by artifacts of the preparation process.

Tinland et. al. employed atomic force microscopy (AFM) in an elegant way to map surface pore morphologies of agarose gels in their native hydrated states[90, 91]. But in order to successfully apply this method, a large number of individual pores must be serially scanned to generate a statistically significant ensemble. A favorable combination of experiment parameters must also be identified that will allow the AFM tip to accurately resolve the pore morphology without exerting an excessive contact force that could damage the gel.

4.2 Background

4.2.1 TEM

It has proven difficult to obtain a visual representation of the nanoscale pore architecture in polymer hydrogels. Electron microscopy techniques are widely used to characterize the morphological features of porous materials, with scanning (SEM)

methods[92] capable of probing surface topologies at micron to sub-micron scales and transmission (TEM) methods allowing nanometer-scale resolution of the internal structure. But these techniques cannot be used to image hydrogel samples under native hydrated conditions, making it necessary to employ potentially damaging freeze drying and cryofixation protocols. A further challenge is that the inherently high porosity of hydrogel materials makes it difficult to obtain sufficient contrast to distinguish the underlying polymer network. Consequently, protocols like replica casting have been devised whereby freeze dried gel samples are used as templates over which rigid thin films are subsequently deposited (e.g., platinum and carbon) that mirror the surface pore structure and can be more clearly imaged[51, 93].

Ruchel et al prepared the polyacrylamide hydrogels with the above replica method and studied the morphology change with monomer/crosslinker concentration with TEM. The images of the replica showed that the pore size is inversely proportional to the %T of the hydrogels and structural units have a minimum size at about 5 %C. However their image resolution is relatively low (about 200 nm), making it difficult to distinguish nanoscale details of the structure of the hydrogel. Hsu etc investigated the polyacrylamide with the same cryo and replicate technique and showed that most of the pores of polyacrylamide are around 95 Å or bigger, with some between 95 Å and 60 Å. While data from these experiments allow qualitative trends to be inferred, the

indirect nature of these TEM methods combined with lingering uncertainties about the detrimental effects of cryopreparation make quantitative interpretation difficult. Also it is difficult to get any information about the inner structure and morphology of the material because only surface features are imprinted on the replicate. In addition, expensive cryo equipment is often not available and the sample preparation procedure is very tedious and time consuming. Moreover; the pores in hydrogels may fracture and be destroyed by ice in the pores.

These experimental challenges highlight a need for characterization techniques that are more suitable for use with hydrogel samples so that the interplay between their pore morphology, mechanical response, and transport characteristics can be better understood. Here we employ a sample preparation method based on a variation of critical point drying that allows water to be gently displaced from the hydrogels under ambient conditions[94]. Additionally, significant contrast enhancement is achieved by staining the samples with ruthenium vapor prior to mounting them on TEM grids. This procedure has enabled us to directly image the pore morphology in photoinitiated crosslinked polyacrylamide / bis-acrylamide hydrogels without the need to employ any cryo-preparation steps.

4.2.2 Rheology

A material's viscoelastic response can be expressed in terms of the phase difference δ between stress and deformation (strain) through a storage modulus (in-phase component) $G' = (\sigma^0/\gamma^0)\cos\delta$ and a loss modulus (out of phase component) $G'' = (\sigma^0/\gamma^0)\sin\delta$, where σ^0 and γ^0 are magnitudes of the stress and strain respectively. During photopolymerization, G' increases rapidly with time after the onset of gelation until an equilibrium plateau is reached (Figure 4.4, $G'' << G'$; typically less than 0.5% of G'). In this regime, rubber elasticity theory suggests that the shear modulus can be described by $G \sim G' = nRT$, where n is the number density of active crosslink junction points (mol/m^3) and G' is the plateau value of the storage modulus. A length scale representative of a characteristic pore size can then be inferred from the crosslink density by assuming that all crosslinks contribute to elastically active junctions and that these junctions are dispersed uniformly throughout the gel. In this picture, the length scale $L = (1/nN_A)^{1/3} = (RT/G'N_A)^{1/3}$ emerges as an estimate of the average pore diameter.

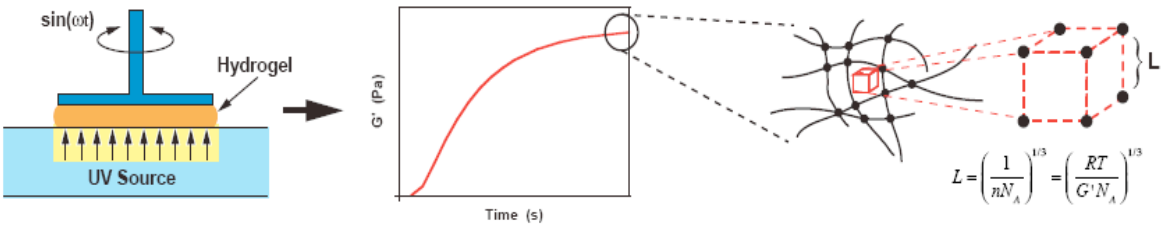

Figure 4.4 Illustration of the pore size measurement using rheology. Mechanical measurements based on small amplitude oscillatory shear allow the evolution of the storage (elastic) modulus G' to be measured during photopolymerization, after which the crosslink density can be determined from rubber elasticity theory and used to extract a length scale that represents the average pore size.

4.2.3 DSC

Thermoporometry is a technique that enables pore size information to be extracted from differential scanning calorimetry (DSC) data by examining the melting point depression associated with water confined along the interior surfaces of a hydrated porous material (Figure 4.5)[95]. The physical principal is similar to conventional intrusion-based methods and involves considering the interplay between the equilibrium temperature at which solid and liquid phases of water coexist within the pores and the interfacial curvature between phases. Since the shape of this interface depends on the pore size and geometry, a relationship can be derived that connects the

shift in the melting transition temperature ΔT observed in a DSC experiment to a characteristic pore radius r_p [96]. It is typically assumed that the pores are cylindrically shaped, in which case a relationship can be obtained that is either theoretically based[95] or obtained semi-empirically by correlating the temperature shifts observed in a series of monodisperse samples of varying pore size[97-99]. Brun etc[95] theoretically derived a reciprocal dependence between the temperature shift and the pore radius when using water and benzene as the probe liquid.

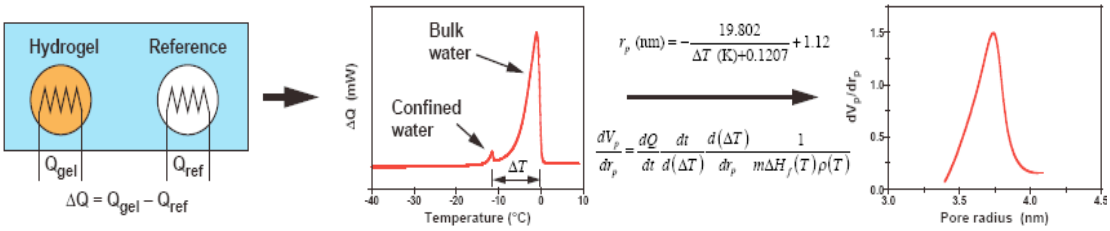

Figure 4.5 Illustration of the pore size measurement using DSC. Thermoporometry methods use DSC to measure a temperature shift ΔT in the heat flow curve corresponding to melting of water confined within the hydrogel pores. The magnitude of this shift can be related to the average pore radius r_p (ΔT is negative here), and the shape of the shifted transition peak can be related to the pore size distribution expressed in terms of a differential pore volume dV_p/dr_p.

The physical principal of thermoporometry is similar to conventional intrusion-based methods and involves considering the interplay between the equilibrium temperature at which solid and liquid phases of water coexist within the pores and the interfacial curvature between phases. In the absence of monodisperse hydrogel samples, we have found that the relationship (equation 4.1), formulated based on temperature shift data observed in hydrated controlled pore glass[97], yields pore sizes that are in most consistent agreement with our rheology and TEM measurements.

$$r_p = \frac{19.082}{\Delta T(K) + 0.1207} + 1.12 \qquad (4.1)$$

The pore size distribution can also be quantitatively determined by relating the shape of the thermal transition peak in the DSC heat flow curve to the fraction of confined water undergoing phase transition at a given temperature. This analysis leads to an expression in terms of a differential pore volume dV_p/dr_p and the DSC scanning rate $d\Delta T/dt$ that takes the form

$$\frac{dV_p}{dr_p} = \frac{dQ}{dt}\frac{dt}{d(\Delta T)}\frac{d(\Delta T)}{dr_p}\frac{1}{m\Delta H_f(T)\rho(T)} \qquad (4.2)$$

where dQ/dt is the DSC heat flow signal expressed in units of power (mW), m is the mass of the dry gel, and ΔH_f and ρ are the heat of fusion and density of the bulk water[100]. Thermoporometry is a potentially powerful characterization tool for hydrogel systems[101, 102] because measurements can be made directly in the hydrated state,

eliminating the need for sample preparation procedures that could distort the pore network (e.g., freeze drying).

One advantage of thermoporometry is that no extra sample preparation is needed as water is used as the probing liquid and hydrogels are measured in their original state during the experiments. Another advantage is that not only the pore size, but also the pore size distribution of the hydrogels can be derived from the DSC experiment. At present most of the research is focused on the CPG (controlled pore glass) and polymer membranes with few studies examining the water-imbibed hydrogel systems. Also many different equations have been developed to calculate the pores size of the porous materials[95, 97-99]. In this session, we will measure the pore size and pore size distribution of the water imbibed hydrogels with thermoporometry and compare the different temperature shift calculation methods and equations to find the best equation suitable for hydrogels.

4.2.4 Drug delivery

Hydrogels are widely used transport vehicles for drug delivery due to their biocompatibility and physiochemical properties. Hydrogels can swell in water or biological fluids enabling drugs or proteins trapped inside to be released and diffuse out of the crosslinked network. The interplay between a hydrogel's nanoporous morphology and its transport characteristics is especially evident in these applications

where kinetics associated with controlled release of small molecule payloads are closely correlated with the network's characteristic pore size[6-9].

4.3 Objective

1. First we would like to develop a series of standard rheology, DSC, TEM experiment protocols that can be implemented on a routine basis to study the porous morphology of not only hydrogels but also other similar biomaterials whose pore sizes are also difficult to characterize.
2. Second, we would like to obtain a detailed picture of the hydrogel nanosacle pore morphology and understand how it can be manipulated so that we can rationally identify hydrogel formulation and synthesis conditions best suited for a specific application.
3. Third, we would like to explore the influence of polydispersity and porous morphology on the properties and applications of the material. For example, what is the property difference between two hydrogels with the same pore size and different polydispersity. Few people have investigated these issues.

4.4 Materials and methods

4.4.1 Hydrogel preparation

Crosslinked polyacrylamide hydrogels were polymerized from a solution of

powdered acrylamide monomer and bis-acrylamide crosslinker with ammonium persulfate (APS) as the initiator. Stock solutions of photopolymerizable gel formulations were prepared by combining monomer and crosslinker in deionized water to obtain the desired concentration. Immediately prior to each experiment, 2 μL of a freshly prepared 1 % w/v aqueous APS solution was added to 2 mL of the gel stock solution and gently mixed. Hydrogel disks (~180 μL in volume) were polymerized in the parallel plate fixture of a rheometer fitted with a UV curing stage (see description of rheological experiments) in order to allow G' (and hence the average pore size) to be measured during the crosslinking reaction. Following nomenclature used in gel electrophoresis literature [41, 42](these hydrogels are routinely used as sieving matrix media for electrophoretic separations of DNA and proteins), we express gel concentrations in terms of the monomer concentration ($\%T = \frac{m_{AAM}(g) + m_{CL}(g)}{V_{solution}(mL)} \times 100$) and crosslinker concentration ($\%C = \frac{m_{CL}(g)}{m_{AAM}(g) + m_{CL}(g)} \times 100$), where AAM denotes the acrylamide monomer and CL denotes the bisacrylamide crosslinker.

4.4.2 TEM experiments

Hydrogel disks polymerized in the rheometer were cut into fine pieces on a glass wafer using a thin blade. Several drops of water were added to the gel pieces in order to create a mixture with a liquid-like consistency. Next, vapor staining was performed by mixing 20 mg of Ruthenium (III) chloride hydrate and 1 mL of sodium hypochlorite

solution (10%) in a small pan and placing it beside the hydrogel sample in a small sealed vessel for 5–8 min. TEM grids were cleaned by glow discharge, after which a 1–2 μL aliquot of the stained gel solution was pipetted over the surface. The grids were successively immersed in liquid nitrogen, methanol, and hexamethyldisilazane for 30 s each with gentle agitation at each step, then dried overnight under ambient conditions in a fume hood with filter paper positioned between forceps points to absorb excess solvent. HMDS is a well-known and extremely gentle alternative to CO_2-based critical point drying, even capable of preserving the integrity of biological specimens to permit subsequent DNA extraction and PCR[103]. The dried grids were then coated with a thin carbon film (1 – 5 nm) to protect the polymer surface from the electron beam. Clearest images were obtained at locations near edges of the sample where the gel is thin enough so that there is minimal overlap between multiple dark stained layers (regions that are too thick appear as opaque dark spots).

Osmium staining was also employed but was later abandoned due to several complications. First, the staining process for osmium is much slower (usually about 12~24 hours) while the Ruthium staining only takes around 5 minutes. Second, the hydrogel itself may swell or dry during the long staining process. Third, the extent of staining is hard to control in osmium due to not so obvious color change in the sample. This is important because the objective is to apply enough staining to acquire sufficient

contrast, while not so much that the gel structure become too dark and distorted.

Critical point drying methods using carbon dioxide[104] were also tried but we found that the hydrogel samples became easy contaminated by impurities from the equipment (such as the porous specimen holder made of chalk). The hydrogel sample was also found to become severely distorted after the process. The method of embedding the polymer in an epoxy material was also tried, however the thin ultramicrotom sections break very easily in the water reservoir, making it difficult to load them on the grids.

Images were obtained using a JEOL JEM-2010 200kV high-resolution TEM instrument. Quantitative analysis of the TEM images was performed using the open source software package *ImageJ*. Images with clearly distinguishable light- and dark-colored regions were selected so that no further adjustments (contrast enhancement, etc.) were needed. For analysis purposes, we defined the pores as consisting of light regions that were bounded by a darker stained perimeter. Pore diameters were estimated by measuring the size of each light-colored region in units of pixels (two measurements were taken and averaged) and calibrating the result against a known size standard (e.g., SiC_4) to obtain units of length. We chose to exclude pores whose diameters were measured to be larger than 100 nm because at that scale it became difficult to determine whether these regions represented actual features of the pore network or were artifacts of sample cleavage near the edges (these outliers only represented a small fraction of the

total ensemble). Finally, data from multiple images were combined until an ensemble of at least 1,000 measurements was obtained from which a histogram of the pore size distribution could be constructed.

4.4.3 Rheology experiments

Small amplitude oscillatory shear experiments were performed using a Parr-Physica MCR-300 rheometer with a 25 mm diameter parallel-plate geometry. A UV curing fixture was used that incorporated a transparent lower plate to illuminate the sample using an EXFO Omnicure 1000 UV source. All polymerization reactions were performed at 20 °C, and a solvent trap was used to minimize evaporation. Measurements were performed at an amplitude of γ^0=0.01 and an angular frequency of ω=1 rad/s. Gels were polymerized under UV illumination for 50 min to ensure that the reaction ran to completion. These experiments are straightforward to perform and, when combined with the use of photopolymerization, allow the evolution of a hydrogel network to be probed in-situ during the course of the crosslinking reaction.

4.4.4 Thermoporometry experiments

Measurements were performed using a Perkin-Elmer Pyris-1 DSC instrument equipped with a liquid nitrogen cooling accessory. Prior to the experiments, the crosslinked hydrogels were rinsed in deionized water to remove residues. Hydrogel

samples (10-20 mg) were then cut and sealed inside aluminum DSC pans with an added 1–2 mg excess of bulk water. During each experiment, the temperature was first decreased to –40 °C and held for 15 min for freezing after which the sample was heated to 15 °C at a rate of 2 °C/min using an empty sealed pan as reference. After the experiments, the pans were punctured and dried under vacuum at 25 °C to determine the polymer and water content of each sample. Temperature shifts were quantified using the difference between temperature at the confined water peak and the onset of the bulk water peak[97].

4.4.5 Release experiments

Hydrogel disks were polymerized in the rheometer as described above. Water uptake was measured by immersing the disks in deionized water and allowing them to fully swell for 2–3 days after which the gels were weighed, dried under vacuum at room temperature for at least 3 days, and weighed again. In this way, the extent of water uptake could be determined from the masses of the swollen m_s and dried m_d samples (% Uptake = $[(m_s - m_d)/ m_d] \times 100$). Prior to release experiments, hydrogel disks were loaded by imbibation in a concentrated aqueous solution containing one of the molecular species of interest. The species tested consisted of small dye molecules Rhodamine B (MW = 479 Da; 1.0 g/100 mL) and Rose Bengal (MW = 1018 Da; 1.0

g/100 mL), as well as bovine serum albumin (MW = 66 kDa; 0.2 g/mL) and a 20 base single-stranded DNA oligonucleotide (sequence GAA GAG CCA AGG ACA GGT AC; 540 ng/μL). We opted to load the gels by imbibation after they were polymerized because we did not want to introduce the possibility of altering the hydrogel morphology due to the presence of these species during the crosslinking reaction.

Polymerized gel disks were first dried and weighed to obtain the mass of the polymer m_{poly}. Next, the dried disks were immersed in the dye solutions for at least 3 days (or one week for the DNA solution) and weighed again to obtain the combined mass of the polymer and dye solution $m_{poly+dye+water}$. This allowed the mass of the dye solution to be determined from $m_{dye+water} = m_{poly+dye+water} - m_{poly}$, after which the mass of the dye alone could be extracted using the mass concentration of the prepared dye solution and assuming that the dye concentration in the gel was the same as in the dye solution ($m_{dye} = m_{dye+water} \times [m_{dye}/m_{dye+water}]_{\text{in prepared dye solution}}$). Finally, the amount of loading was calculated from the ratio between the masses of the dye and polymer (Amount of Loading (wt %) = m_{dye}/m_{poly}).

After loading, the disks were removed and carefully blotted dry, then placed in 10 mL of water. Aliquots of the liquid surrounding the hydrogels were sampled at regular time intervals and absorbance was measured using a NanoDrop ND-1000 spectrophotometer at wavelengths corresponding to the absorbance maximum for each

species (Rhodamine B: 555 nm, Rose Bengal: 548 nm, DNA: 260 nm), after which each gel disk was placed in a fresh 10 mL volume of water. Absorbance values were converted to concentration by constructing calibration curves from absorption measurements of solutions of each species prepared at known concentrations. The mass of dye released at each measurement time was determined by multiplying the measured concentration by the volume of water in which the hydrogel disk was immersed (10 mL), and measurements continued until dye released at each stage was no longer detectable. The cumulative release at the N^{th} measurement time was calculated from the ratio of the total mass of dye released up to that point $\sum_{N} m_i$ to the mass of dye initially in the gel m_{dye} determined from the amount of loading as described above (Release Percentage (%) = $\sum_{N} m_i \ / \ m_{dye}$).

4.5 Characterizing the porous morphology with TEM

The TEM images reveal a morphology characterized by a distribution of lightly shaded regions corresponding to open pores that are interspersed between dark areas attributable to the stained polymer. TEM pictures of 9 %T-9 %C are shown in Figure 4.6 and give us a bird view look at a large area of the polymer at a lower magnification (Fig 4.6 a, the scale bar is 100nm). Most of the pores in the pictures have similar size and shows no sign of two distinct categories of large pores and small pores suggested by the bimodal theory. As we increase the magnification and zoom in, we can see that

the pores of the gel are evenly dispersed within the gel and some fracture of the polymer might appear due to the sample preparation (Fig 4.6 b, the scale bar is 50 nm). The pore shape and structure of the hydrogels can be clearly and directly visualized at even higher magnification (Figure 4.6 c, the scale bar is 20 nm). It is clear that the pores of the hydrogels are not strictly round and have oval or other irregular shapes. The sizes of the pores are not the same and have a distribution.

Upon increasing either the monomer or crosslinker concentration (following the nomenclature in electrophoresis literature, we express these parameters in terms of %T and %C respectively), a progression is evident from a polydisperse ensemble of highly irregular pore shapes and dark stained polymer clusters at low concentrations toward a more uniformly distributed morphology at higher concentrations with pores that display much less asymmetry. This progression is consistent with the formation of bundled clusters of higher molecular weight polymer chains at low crosslinker concentrations, ultimately evolving toward a more homogeneous network with less polydispersity in pore size at higher concentrations when more monomer and/or crosslinker molecules are available during polymerization.

(a)

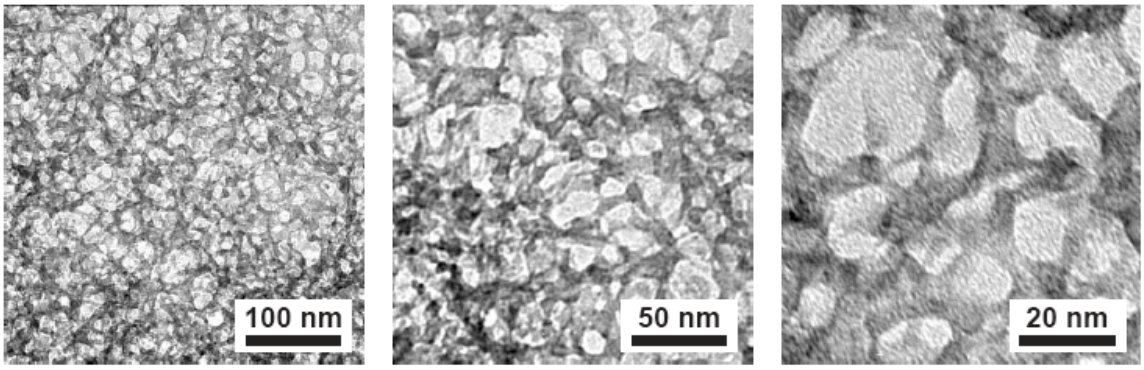

Figure 4.6 Evolution of pore morphology with hydrogel composition. (a) TEM images of 9 %T-5 %C polyacrylamide hydrogels at 50k, 100k, 200k magnifications. Lightly shaded regions correspond to open pores, darker areas indicate stained polymer. (b) TEM image sequence depicting how highly irregular pore shapes and dark stained polymer clusters at low concentrations toward a more uniformly distributed morphology at higher concentrations with pores that display much less asymmetry. This progression is consistent with the formation of bundled clusters of higher molecular weight polymer chains at low crosslinker concentrations, ultimately evolving toward a more homogeneous network with less polydispersity in pore size at higher concentrations when more monomer and/or crosslinker molecules are available during polymerization. The morphology changes with monomer (%T; increasing from top to bottom) and crosslinker (%C; increasing from left to right) concentrations. A polydisperse pore architecture is evident at low concentrations, progressing toward a more homogeneous network at higher concentrations. Scale bar, 50 nm.

(b)

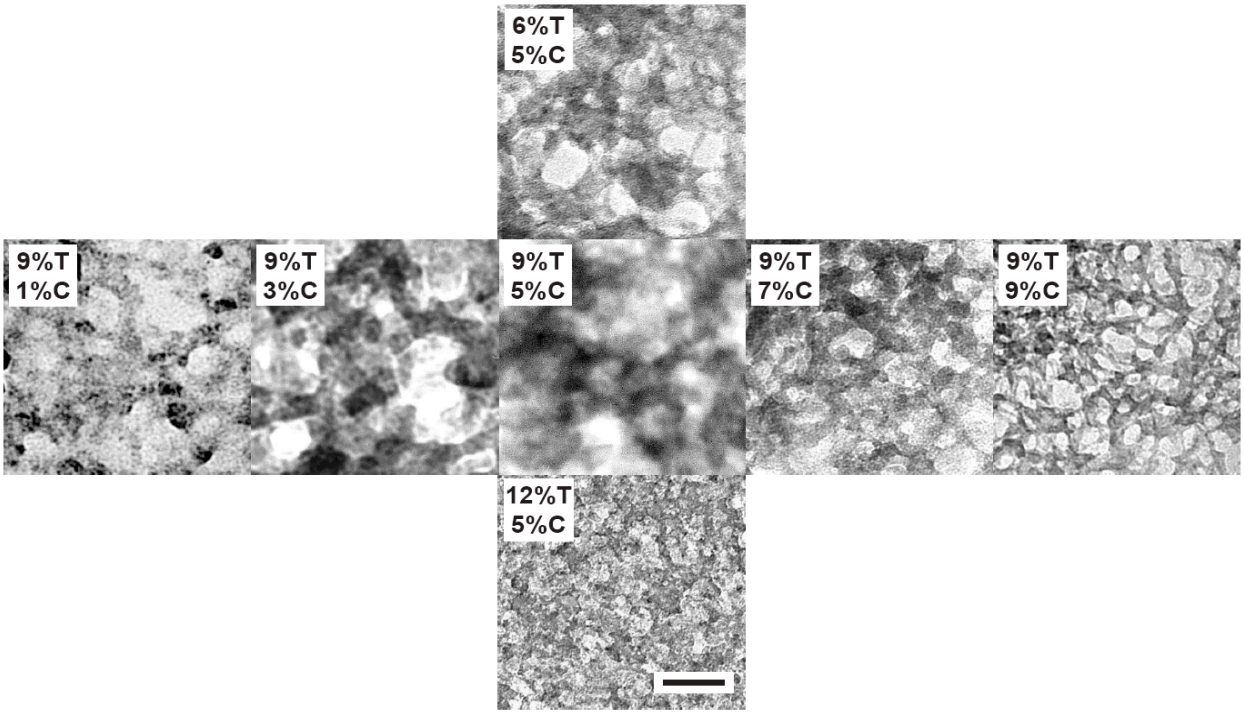

Figure 4.6 Continued

We also obtained quantitative characterization of the pore size distribution using analysis of an ensemble of pores from multiple TEM images. The diameter of each pore in the pictures is carefully measured two times in different angles and at least 1,000 pores were analyzed for each different hydrogel. All measured diameters of the pores are accumulated to generate a histogram and the obtained pore size and distribution of hydrogel are shown in Figure 4.7. The pore size and pore size distribution measured from TEM images are very similar to those from DSC experiments. These results are also consistent with the qualitative observations of smaller mean pore sizes and less polydisperse pore size distributions with increasing monomer and crosslinker concentration. The pore size and pore size distribution measured from TEM also do not display signatures of a sharply bimodal pore size distribution[87] (i.e., incorporating populations of two distinctly different pore sizes).

(a)

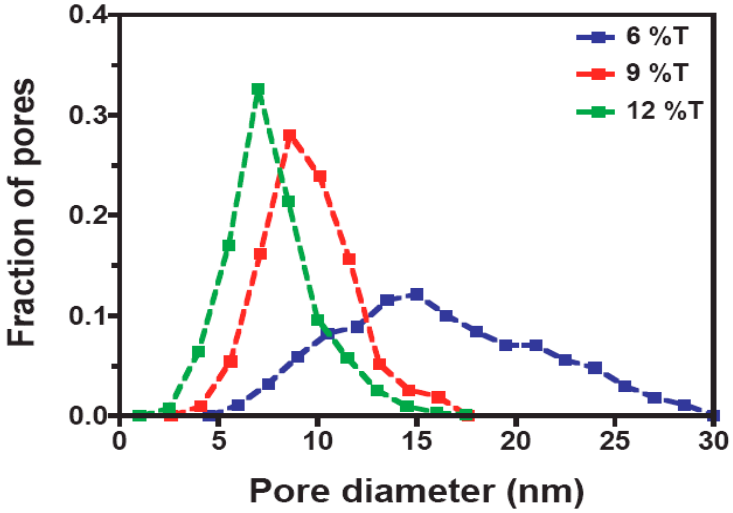

(b)

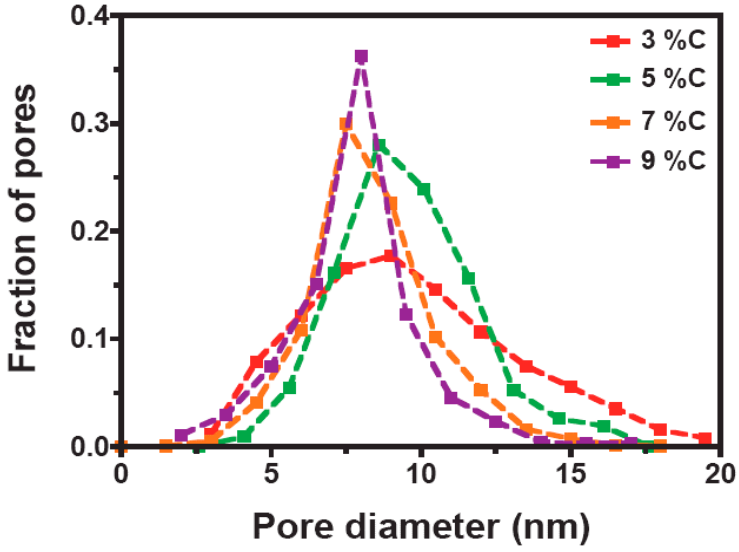

Figure 4.7 Fractional pore size distributions determined from analysis of TEM images (ensembles of at least 1,000 pores were measured). (a) Effect of monomer concentration (5 %C gels polymerized at 325 mW/cm^2) (b) Effect of crosslinker concentration (9 %T gels polymerized at 325 mW/cm^2).

4.6 Characterizing the porous morphology with rheology

When we apply this rheological approach to examine the influence of monomer and crosslinker concentration on hydrogel pore size, a key trend that becomes evident is a decrease in the mean pore diameter by a factor of two (from about 12 to 6 nm) as the monomer concentration is increased from 6 to 12 %T (Fig. 4.8 a). A similar but less pronounced decrease in average pore size is also evident with increasing crosslinker concentration (%C) and UV illumination intensity during polymerization (Fig. 4.8 b, c). These qualitative trends are consistent with the TEM images in Fig. 4.6, as well as pore size estimates derived from electrophoretic mobility measurements in similar photopolymerized hydrogel formulations[105]. Electrophoretic mobility studies in hydrogels formed by chemically initiated polymerization indicate the presence of somewhat larger pores[106], further highlighting the influence of reaction conditions (or even the electrophoresis process itself) on the gel nanostructure.

(a)

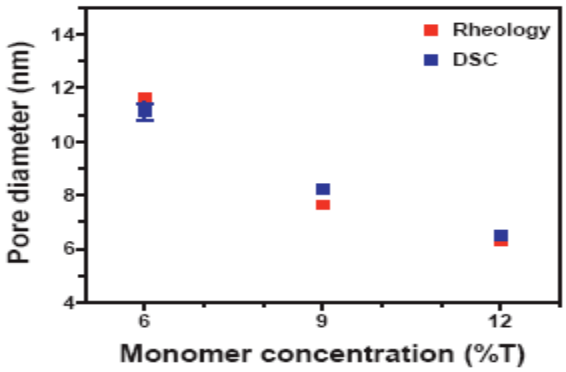

(b)

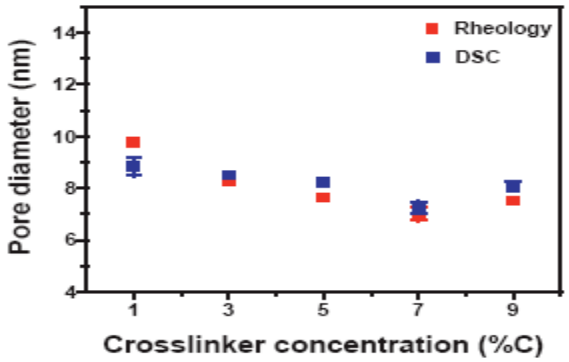

(c)

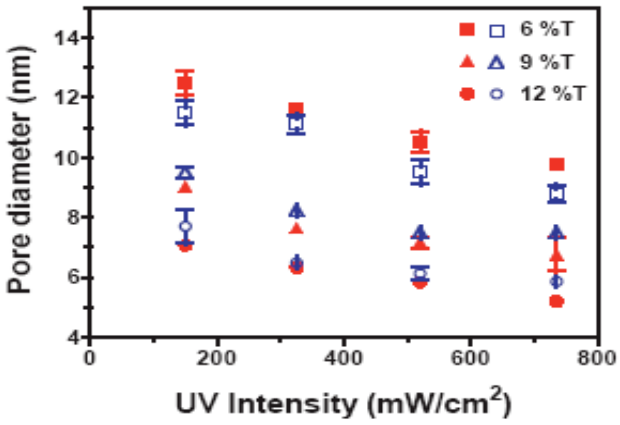

Figure 4.8 Comparison of pore sizes derived from rheology and DSC. Rheology and DSC data are compared with different (a) monomer concentration %T (b) crosslinker concentration %C (c) UV intensity.

4.7 Characterizing the porous morphology with DSC

The DSC curve of pure water is shown in Figure 4.9 (a). There is only one large peak around 0 °C in the heat flow curve. A typical DSC heat flow curve of hydrogels is shown in Figure 4.9b with two peaks in the heat flow curve. After comparing the peaks of pure water and the hydrogels, it is clear that the smaller peak around –10 °C is caused by water confined within the pores of the hydrogel, and the larger peak around 0 °C represents the bulk water.

The temperature depression, defined as T-T_o, is the most important parameter in thermoporometry and can be calculated in different ways. It is common to take T as the peak temperature of the confined liquid and T_o as 0 °C without regarding the real bulk water peak temperature when water is the probe media[95, 98, 99, 101, 107-110]. However the peak temperature of bulk water often deviates from 0 °C and is seldom exactly at 0 °C. Landry[97] studied the DSC curves of the controlled pore glass in water and compared different ways to calculate the temperature depression such as ΔT_{pk} (two peak temperature difference), $\Delta T_{on\text{-}pk}$(peak and onset temperature difference), ΔT_{on} (onset temperature difference). $\Delta T_{on\text{-}pk}$ and ΔT_{on} are more consistent than ΔT_{pk} when the heating rate and liquid to porous-solid ratio vary. Empirical equations were then derived to obtain the pore size from the $\Delta T_{on\text{-}pk}$. In this session, we will measure the pore size and distribution of the water imbibed hydrogel with thermoporometry and

(a)

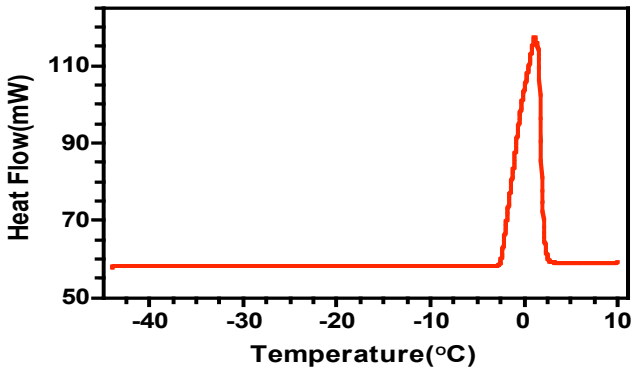

(b)

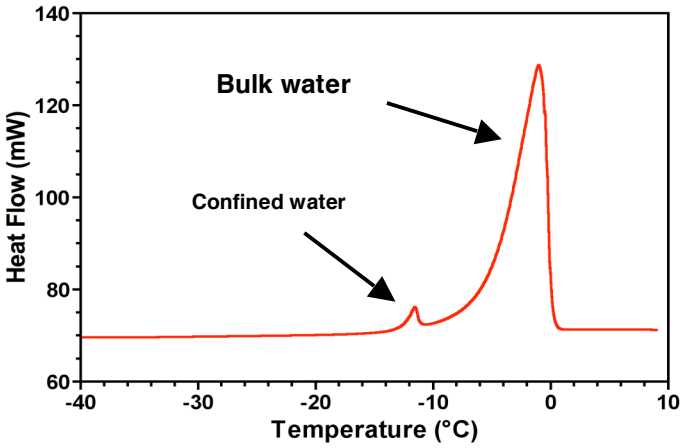

Figure 4.9 The DSC heat flow curve of (a) pure water (b) 12 %T-5 %C hydrogels polymerized at UV intensity of 325 mW/cm^2.

compared the different temperature shift calculation methods and equations to find the best equation suitable for hydrogels.

The temperature difference between peaks can be determined in different ways and the methods used will directly influence the calculated value of pore size and distribution. We compare the three main methods: ΔT_{on-pk} [97], T_0 [95], ΔT_{pk} [98], in Figure 4.10

$$r_{p(}(nm) = -\frac{19.08}{\Delta T + 0.1207(K)} + 1.12 \quad \text{(Reference 97)} \qquad (4.1)$$

$$r_{p(}(nm) = -\frac{32.33}{\Delta T(K)} + 0.68 \quad \text{(Reference 95)} \qquad (4.3)$$

$$r_{p(}(nm) = -\frac{33.3}{\Delta T\ (K)} + 0.32 \quad \text{(Reference 98)} \qquad (4.4)$$

The measured pore size using ΔT_{on-pk} is very similar to the pores derived from other methods and the value of ΔT_{on-pk} changes little with experiment conditions such as heating rate[97]. In our experiments ΔT_{on-pk} and the Landry equation (equation 4.1) will be used to characterize the pore size of the hydrogel. The pore size distribution is derived from equation 4.2 and then normalized to get the final distribution.

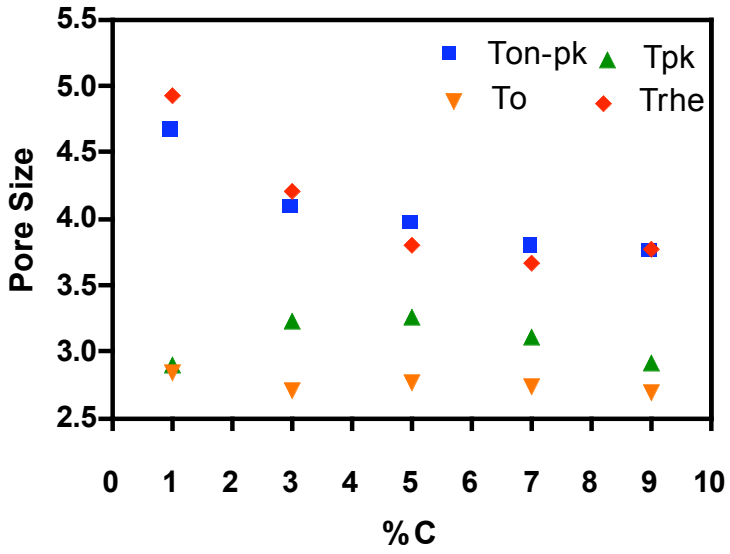

Figure 4.10 Pore size derived from different temperature measurement method, techniques and equations.

Finally, FWHM (Full Width at Half Maximum) is defined as difference between the two extreme values of the independent variable at which the dependent variable is equal to half of its maximum value. It is employed to quantitatively study the breadth of the pore size distribution.

A series of experiments were performed to study the pore size and distribution change with %T, %C, UV intensity. The pore size of the hydrogel decreases with increasing %T and the distribution became narrower at the same time (Figure 4.11 a). This means that the pore size of the hydrogels became more monodisperse with higher monomer concentration. This is also confirmed by the FWHM data in Figure 4.11b.

(a)

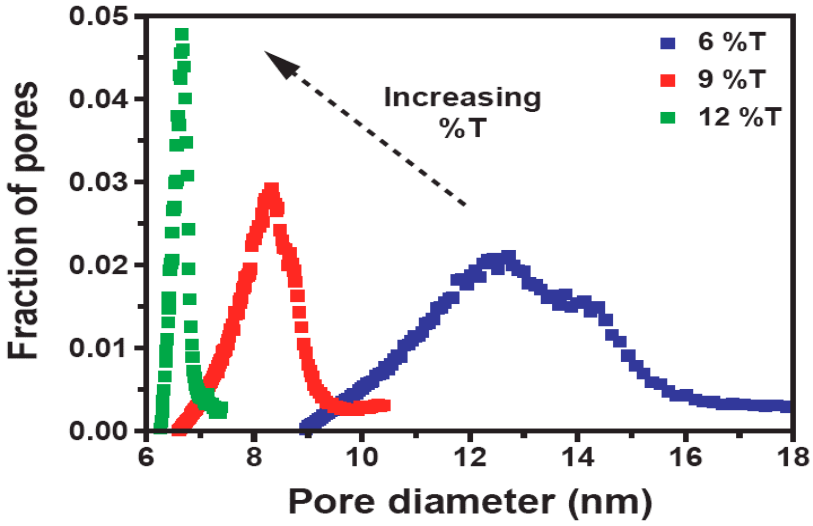

(b)

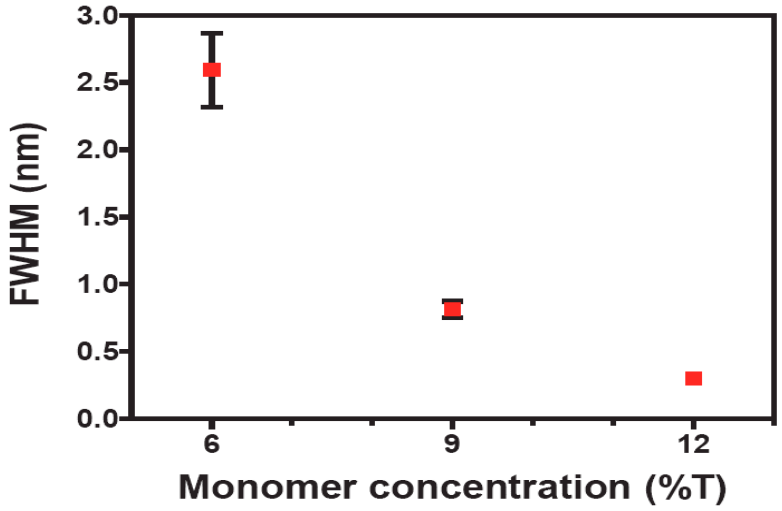

Figure 4.11 Influence of monomer concentration on the pore size distribution of 5 %C gels polymerized at 325 mW/cm^2. (a) Fractional pore size distribution determined by normalizing differential pore volume curves obtained using thermoporometry to unit area and converting the abscissa to units of pore diameter. (b) FWHM data.

The pore size and pore size distribution of hydrogels decreases with increasing crosslinker concentration (%C) until 7%C and reaches a plateau area after that. The evolution has the same trend as the rheology data and is evident in the FWHM data. The evolution is shown in Figure 4.12. The Pore size of the hydrogel also changes with UV intensity as shown in Figure 4.13.The pore size of the hydrogel decrease with increasing UV intensity and the pore size distribution also became narrower at the same time. The stronger UV intensity would enhance the formation of microgels and make them evenly dispersed compared with the lower UV intensity. This would make pores smaller according to the pore definition and at the same time it would be less likely to form too large pores during the polymerization process. The pore size distribution of hydrogels also narrows simultaneously.

(a)

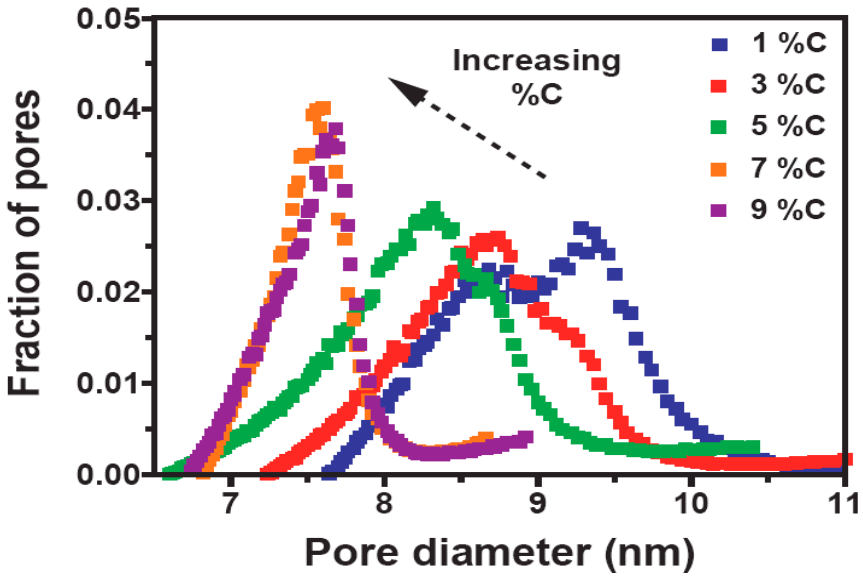

(b)

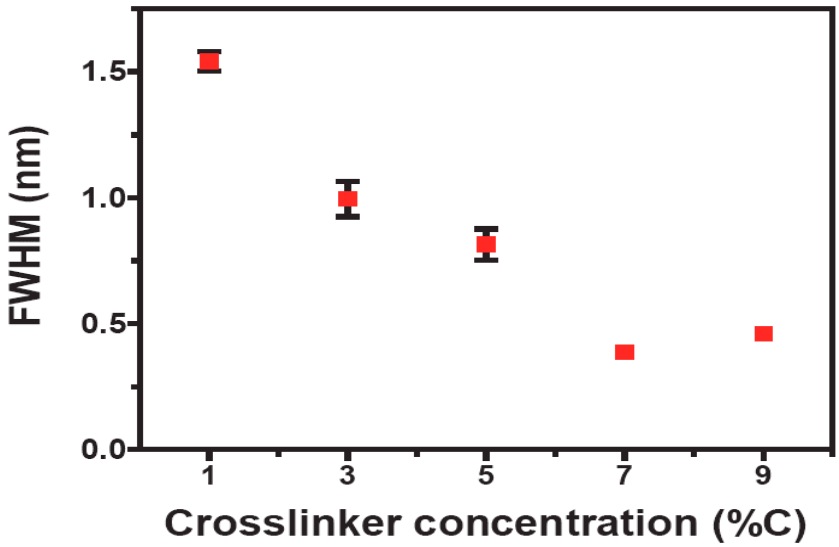

Figure 4.12 Influence of crosslinker concentration %C on the pore size distribution of 9 %T gels polymerized at 325 mW/cm^2. (a) Fractional pore size distribution (b) FWHM data.

(a)

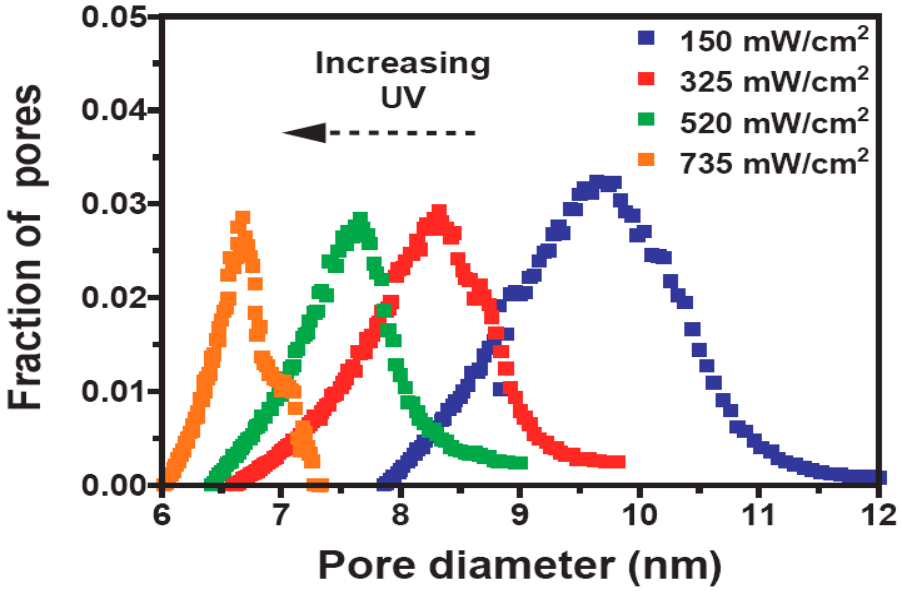

(b)

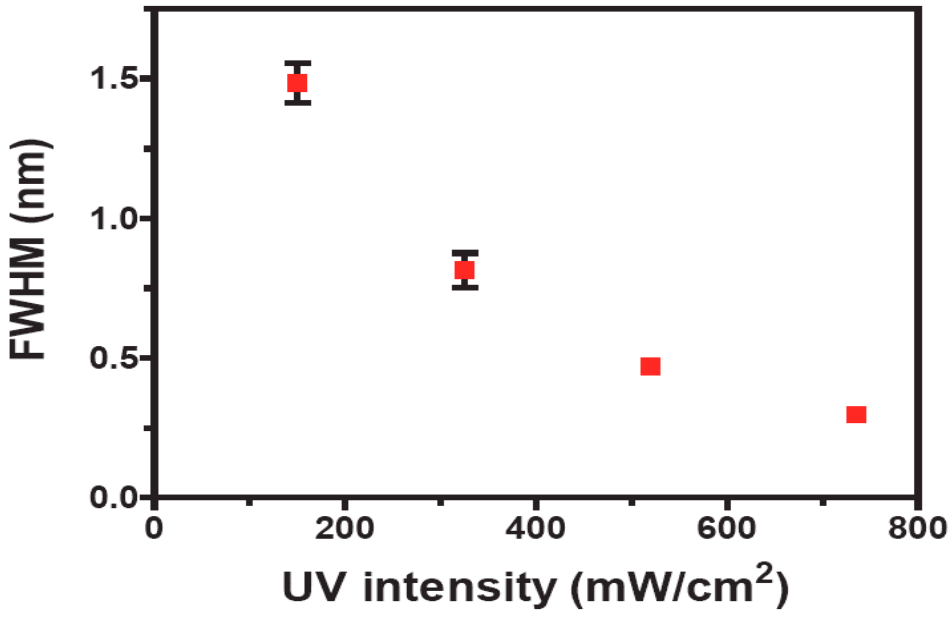

Figure 4.13 Influence of UV intensity on the pore size distribution of 9 %T, 5 %C hydrogels. (a) Fractional pore size distribution (b) FWHM data.

It is interesting to find that some hydrogels may have similar average pore size, but very different range of pore size distribution (Figure 4.14). For example, the 9 %T, 5 %C (under the UV intensity 150 mW/cm^2), 9 %T-3 %C (under UV intensity of 325 mW/ cm^2), 9 %T-9 %C (under UV intensity of 325 mW/cm^2) hydrogel have similar pore size of 4.5 nm, 4.4 nm and 4.3 nm respectively, however their FWHM ranges from 1.3 nm, 0.5 nm to 0.2 nm. Most of the research to date has been concentrated on the average pore size, with few if any studies investigating the pore size distribution.

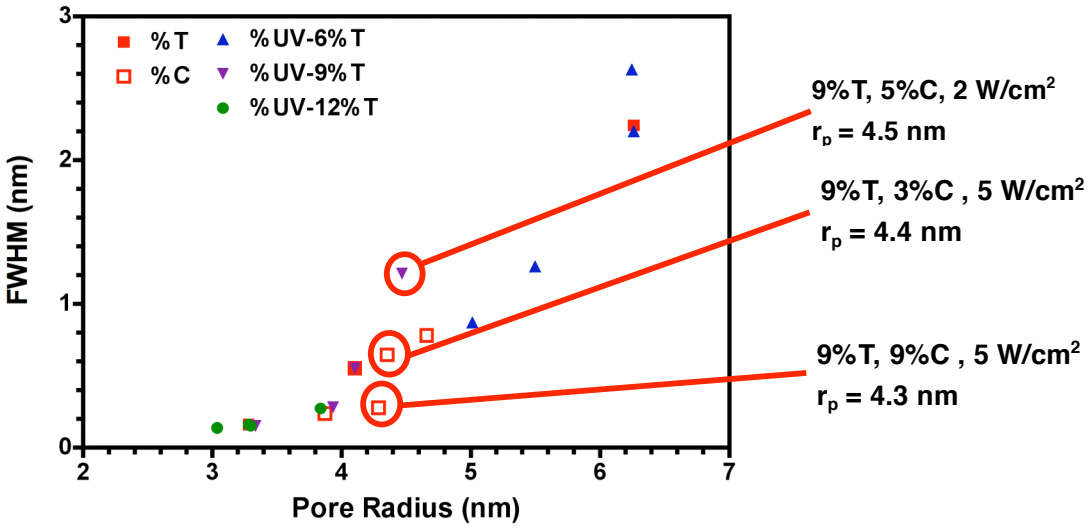

Figure 4.14 FWHM of different hydrogels as a function of pore radius.

The pore sizes of hydrogels derived from rheology, DSC and TEM are compared

and shown in Figure 4.8. The data shows that pore sizes characterized by different methods yield very similar results. We have already shown that the rheology and electrophoresis methods gave similar pore size measurement of the hydrogel. All the results are self consistent and give us confidence that we give a reasonable estimate of the average pore size.

4.8 Release experiments

These complementary characterization methods allow us to establish a unified picture that shows how composition and polymerization conditions influence the nanoporous morphology of crosslinked polyacrylamide hydrogels. A key observation is that the distribution of pore sizes in these materials is inherently polydisperse, and that there can be significant variations in the extent of this polydispersity depending on composition and polymerization conditions. In order to zero-in on the critical role played by the pore size distribution in shaping hydrogel transport characteristics, we applied these characterization methods to identify two gel compositions whose average pore sizes are virtually identical but whose nanoporous networks incorporate significantly different degrees of polydispersity (Table 4.2). In other words, these gels (a 6 %T, 5 %C gel polymerized at a UV intensity of 735 mW/cm^2 and a 9 %T, 1 %C gel polymerized at 325 mW/cm^2) would be indistinguishable if compared solely on the basis of their mean pore size, but our characterization data indicate that their pore

morphologies are actually very dissimilar with the 9%T hydrogel incorporating a much broader pore size distribution (Figure 4.15). A manifestation of these differences is evident in the gels' uptake characteristics where higher water uptake and loading capacities are evident in the 6 %T hydrogel (Table 4.2). Since we observe a similar mass of imbibed species in each gel, the greater loading capacity per unit mass of polymer observed in the 6 %T hydrogel also reflects its lower overall density as compared with the 9 %T gel.

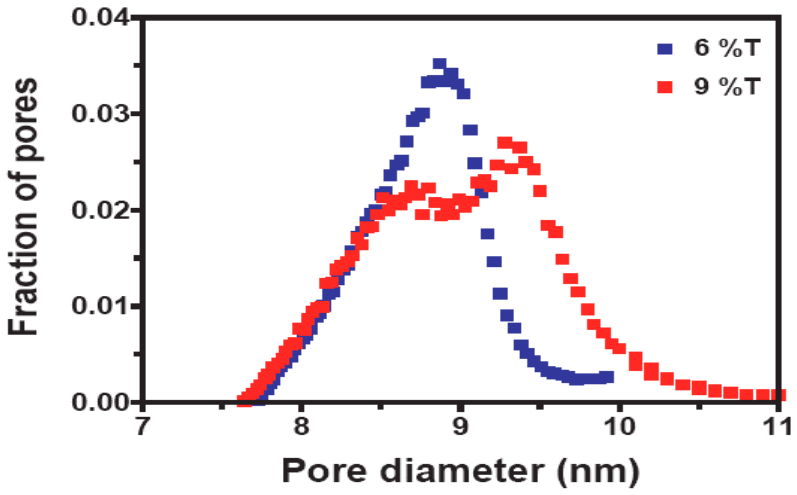

Figure 4.15 Two different hydrogels synthesized under different compositional and polymerization conditions have nearly identical average pore sizes but different pore size distributions as determined by thermoporometry. Pore size distribution of 9%T-1%C (under UV intensity of 325 mw/cm^2), 6%T-5%C (under UV intensity of 735 mw/cm^2).

Table 4.2 Compositional and loading characteristics of hydrogels used in controlled release experiments.

Hydrogel Composition	UV Intensity (mW/cm^2)	Pore Diameter (nm)*	FWHM (nm)*	Water Uptake (wt %)†	Amount of Loading (wt %)†		
					Rhodamine B	Rose Bengal	DNA
6 %T, 5 %C	735	8.80 ± 0.39	0.76 ± 0.18	2240	16.7	19.5	694
9 %T, 1 %C	325	8.85 ± 0.39	1.62 ± 0.12	1350	13.4	16.3	382

* Determined from thermoporometry measurements (mean ± s.d.; computed over an ensemble of 3–5 independent samples).
† Data are the average of 3–4 independent samples.

The influence of polydispersity becomes dramatically evident when we examine release kinetics from these hydrogels loaded with three different molecular species (Fig. 4.16 a-d). Two of the species are macromolecules (bovine serum albumin (BSA) and a 20 base single-stranded DNA oligonucleotide with a characteristic coil diameter of approximately 4 nm[111]) and two are small-molecule dyes (Rhodamine B and Rose Bengal) with diameters in the 1 – 2 nm range[112, 113]. The observed release profiles are characteristic of hydrogels loaded by imbibation, with an initial burst phase attributable to disassociation of loosely trapped molecules near the gel surface followed by a stable sustained phase dominated by transport of molecules from the interior the pore network. Comparing the slopes of the release versus time data reveals that the two gels exhibit markedly different kinetics in the sustained release regime. The more

polydisperse 9%T hydrogel displays faster release (steepest slope) and a greater accumulated release percentage across all species tested. This is especially evident in the DNA and BSA release profiles (Figure 5.25 a, b) where slower kinetics permit these phenomena to be observed with finer temporal resolution. These data suggest that hydrogels incorporating a more monodisperse pore architecture may be best suited to deliver sustained release profiles while more polydisperse networks may be most desirable for rapid release. Although this comparison between gels with significantly different compositions represents a somewhat extreme case where major differences in the pore network architecture would be expected, we emphasize that these two gels would appear identical if compared solely on the basis of their mean pore size using standard characterization methods.

Our experiments reveal that polydispersity in the pore size distribution plays an important role in determining hydrogel release rates, but these effects are generally not captured in conventional characterization approaches based on the mean pore size alone (e.g., swelling methods). We hope the techniques we describe here can become standardized tools to precisely characterize the distribution of pore sizes in hydrogel samples so that we can better understand how the nanoporous morphology is influenced by chemical composition and polymerization conditions. This capability would not only make it possible for polydispersity effects to be considered, but could

ultimately enable these effects to be harnessed to manipulate and tailor a gel's transport characteristics with exquisite precision.

(a)

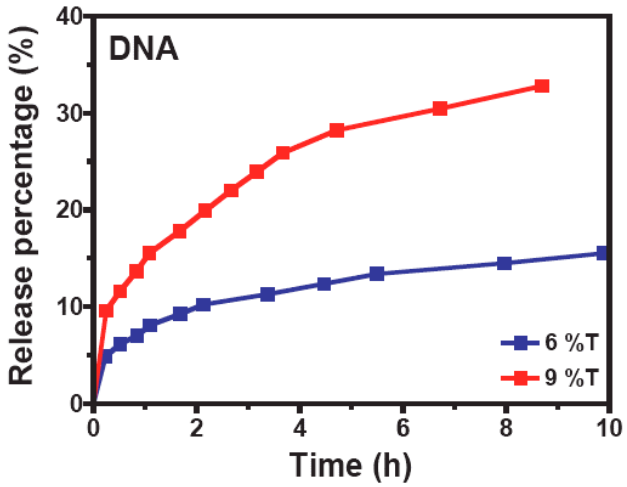

(b)

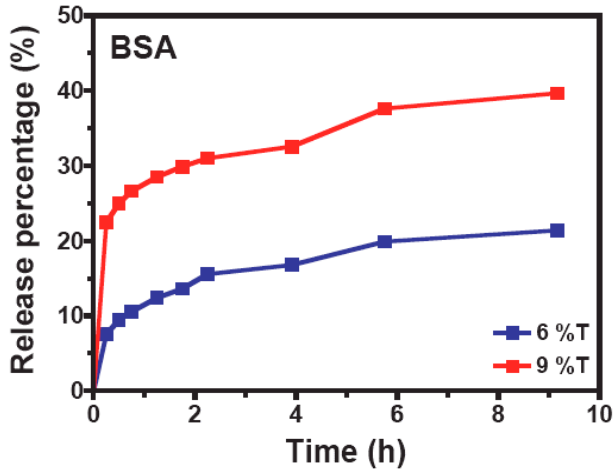

Figure 4.16 Pore size polydispersity strongly impacts hydrogel release kinetics. Cumulative release of imbibed molecular species from the hydrogels in (a) 20 base DNA oligonucleotide, (b) BSA, (c) Rhodamine B and (d) Rose Bengal.

(c)

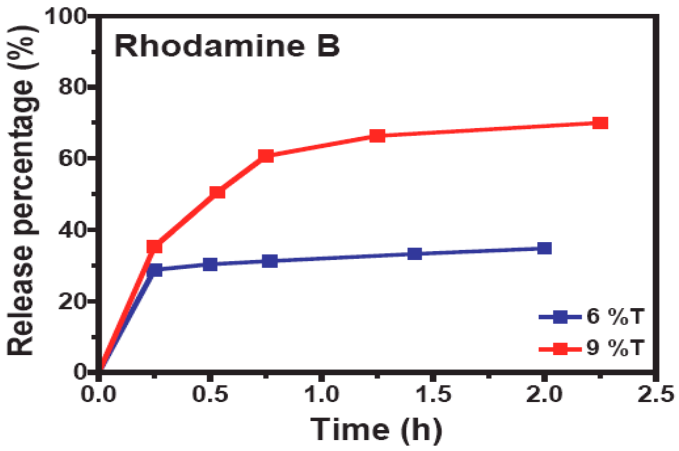

(d)

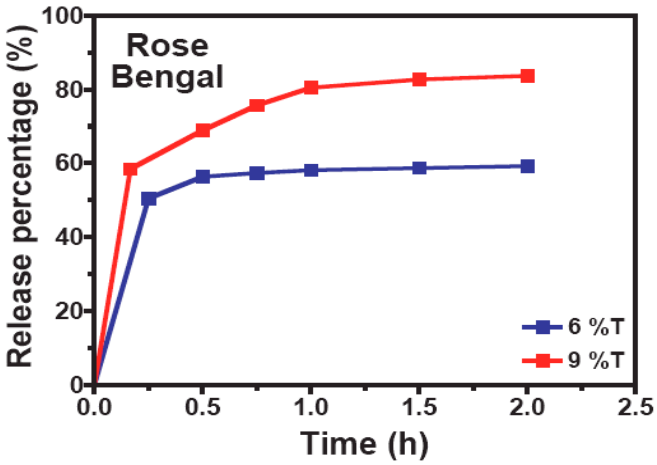

Figure 4.16 Continued

4.9 Conclusions

The broad applications of hydrogels demand increasingly precise and reproducible control over the gel pore network architecture, but the extent of morphological characterization is typically limited to coarse estimates of the mean pore size. Here we show that polydispersity in the pore size distribution plays a critical and previously unappreciated role in directing the controlled release of macromolecules from crosslinked polyacrylamide hydrogels. We demonstrate this by introducing a characterization approach that allows us to identify gels that appear virtually identical when compared on the basis of their mean pore size but display remarkably dissimilar release kinetics owing to differences in their pore size distributions. These results suggest that control of polydispersity offers an unexplored avenue to exquisitely tailor the characteristics of hydrogel-based materials.

5. CONCLUSION AND SUMMARY

5.1 Conclusion

Polyacrylamide hydrogels have a desirable range of pore size that makes them good candidates for applications such as DNA sequencing and protein analysis. However, it is difficult to determine the pore size and its distribution due to large amount of water in the system and the mechanical fragility of hydrogels. Consequently, there are few detailed studies of the interplay between polymerization kinetics, mechanical properties, and the pore structure of hydrogels. In this dissertation, we address this issue using a unique combination of methods that allow us to see the pore morphology in great detail.

In-situ dynamic small-amplitude oscillatory shear measurements were performed during photopolymerization to investigate the evolution of the rheological properties and pore size of hydrogels with UV intensity, polymer composition, and reaction temperature. In a 6 %T hydrogel, the plateau value of the storage modulus G' decreases with increasing UV intensity, while a maximum in the plateau value is observed at a UV intensity of 325 mW/cm^2 for the 9 and 12 %T samples. The value of t_{onset} decreases with increasing UV intensity in all samples. Temperature also exerts an influence on the plateau modulus and gelation onset, although the effect is not as pronounced as that of UV intensity. Doubling the initial monomer concentration in the reaction mixture from 6

to 12 %T increases the plateau value of G' by over an order of magnitude. The average pore size of the hydrogel network was estimated using a simple model based on classical rubber elasticity theory. Despite its simplicity, this model is capable of yielding pore sizes in agreement with those obtained from analysis of DNA mobility during electrophoresis in identical gels.

There is also a lack of studies on the gelation process of hydrogels because of the fast reaction rate, small molecule monomer/crosslinker chemistry and low viscosity and modulus in the system. We found that the photopolymerization reaction stops almost immediately when the UV source is turned off, and this could allow us to obtain critical gel samples "frozen" at exactly the gel point. A polyacrylamide hydrogel system was chosen because its gel point rheological properties have not been extensively studied. The relaxation exponent n decreases with increasing monomer / cosslinker concentration and UV intensity while the corresponding values of gel strength parameter S and the fractal dimension d_f increase under the same conditions. Theses findings suggest the network of the critical hydrogels is strengthened and becomes more tight and elastic with increasing monomer / crosslinker concentration and UV intensity. The modulus G_0 of the polyacrylamide system is much smaller than the plateau values of storage modulus G', and this result is different from what is generally observed in other systems. We find the relaxation

exponent n is connected with the pore size and polydispersity of the material. There exists a linear relationship between the critical gel strength parameter S and the storage modulus of the fully cured hydrogels at all the concentrations and UV intensities we studied. This suggests a key connection between the critical gel and the fully grown polymer network and shows the importance of the critical gel study. Different methods to define the gel point and the respective gel time were also compared.

Thermoporometry is used to measure the pore size based on the melting point depression of water confined in a pore. The average pore size, especially the pore size distribution can be derived from the DSC heat flow curve. Different methods and equations to calculate the temperature depression and pore sizes are compared and one equation is chosen to yield results in closest agreement with the other techniques. The pore size and distribution of hydrogels vary considerably with different UV intensity and crosslinker concentrations.

We present a novel technique to prepare hydrogel samples at room temperature for direct visualization of nanoporous morphology using transmission electron microscopy (TEM). The pore size and pore size distribution of the hydrogels can then be both qualitatively and quantitatively studied. This new preparation technique virtually eliminates freeze fracture effects that often occur in standard preparation protocols and

have made it difficult to image gel pore architectures without damaging them.

In general, the hydrogel pore size and distribution obtained from four different methods are self consistent. The average pore size decreases with increasing UV intensity and monomer concentration %T. There is a maximum of G' value with varying crosslinker concentration while its pore size reaches minimum at the same time. The pore size distribution of polyacylamide hydrogels is relatively narrow and mostly within the range of 5-20 nm.

These techniques help us understand how the nanoporous morphology of crosslinked polyacrylamide hydrogels is influenced by their chemical composition and polymerization conditions. We then examine controlled release of macromolecules from these hydrogels and show that it is possible for gels to appear identical when compared on the basis of their mean pore size, yet display remarkably dissimilar release kinetics owing to differences in polydispersity. These results reveal how the nanoporous architecture of polymer hydrogels shapes their bulk properties, and suggest that the ability to measure and control polydispersity can offer a new and powerful avenue to tailor the characteristics of hydrogel-based materials.

5.2 Summary

In summary this dissertation describes new techniques we have developed that, for the first time, enable both the average pore size and the pore size distribution of hydrogel networks to be quantitatively measured. We demonstrate the importance of these measurements by examining controlled release of macromolecules from crosslinked polyacrylamide hydrogels where we are able to show that it is possible for gels to appear identical when compared on the basis of their mean pore size, yet display remarkably dissimilar release kinetics owing to differences in the distribution of pore sizes they contain. These results are potentially of great importance in biomedical applications (e.g., pharmaceuticals, tissue engineering) because they imply that currently used hydrogel characterization approaches based on measurements of the mean pore size alone (e.g., swelling methods) do not accurately represent the pore network architecture. From a practical standpoint, the experimental methods we describe are an advance over current approaches because they are easy to apply and do not require prior knowledge of any physical material parameters (for which data is often unavailable). Finally, from a polymer physics perspective, our results are of interest because they appear to contradict a long-held and widely accepted viewpoint that the nanoscale pore size distribution is sharply bimodal (based on indirect light scattering measurements dating back to the 1980s).

It is inevitable that polymer hydrogels will possess some degree of pore size

polydispersity, but these effects are generally not considered in conventional characterization approaches based on the mean pore size alone (e.g., swelling methods). This could have important consequences whenever pore size is used as a primary criterion to select hydrogel formulations suitable for a particular application because measurements obtained in this way may not accurately represent the pore network architecture. We hope that the techniques we describe here can become standard experimental tools to quickly and precisely characterize the distribution of pore sizes in hydrogel samples. This capability would not only make it possible for polydispersity effects to be considered, but could ultimately enable these effects to be harnessed to manipulate and tailor a gel's transport characteristics with precision.

REFERENCES

1. Langer, R. & Peppas, N.A. Advances in biomaterials, drug delivery, and bionanotechnology. *AIChE Journal* **49**, 2990-3006 (2003).

2. Peppas, N.A., Bures, P., Leobandung, W. & Ichikawa, H. Hydrogels in pharmaceutical formulations. *European Journal of Pharmaceutics and Biopharmaceutics* **50**, 27-46 (2000).

3. Cushing, M.C. & Anseth, K.S. Hydrogel cell cultures. *Science* **316**, 1133-1134 (2007).

4. Griffith, L.G. & Swartz, M.A. Capturing complex 3D tissue physiology in vitro. *Nature Reviews Molecular Cell Biology* **7**, 211-224 (2006).

5. Albarghouthi, M.N. & Barron, A.E. Polymeric matrices for DNA sequencing by capillary electrophoresis. *Electrophoresis* **21**, 4096-4111 (2000).

6. Burnham, A.S. Polymers for delivering peptides and proteins *American Journal of Hospital Pharmacy* **51**, 210 (1994).

7. Peppas N.A., Mongia N.K. Ultrapure poly(vinyl alcohol) hydrogels with mucoadhesive drug delivery characteristics. *European Journal of Pharmaceutics and Biopharmaceutics* **43**, 51-58 (1997).

8. Shen H-R., Spikes J.D., Kopeeková P., Kopecek J. Photodynamic crosslinking

of proteins. I. Model studies using histidine- and lysine-containing N-(2-hydroxypropyl) methacrylamide copolymers *Journal of Photochemistry and Photobiology B: Biology* **34**, 203-210 (1996).

9. Peterson C.M., Shiah J.G., Sun Y.G., Kopeckova P., Minko T., Straight R.C., Kopecek J. HPMA copolymer delivery of chemotherapy and photodynamic therapy in ovarian cancer *Advances in Experimental Medicine and Biology* **519**, 101-123 (2003).

10. Lutolf M. P, Hubbell J. A. Synthetic biomaterials as instructive extracellular microenvironments for morphogenesis in tissue engineering. *Nature Biotechnology* **23**, 47-55 (2005).

11. Raeber G. P., Lutolf, M.P., Hubbell J. A. Molecularly engineered PEG hydrogels: a novel model system for proteolytically mediated cell migration. *Biophysical Journal* **89**, 1374–1388 (2005).

12. Okay, O., Kurz, M., Lutz, K. & Funke, W. Cyclization and reduced pendant vinyl group reactivity during the free-radical cross-linking polymerization of 1,4-divinylbenzene. *Macromolecules* **28**, 2728-2737 (1995).

13. Naghash, H.J. & Okay, O. Formation and structure of polyacrylamide gels. *Journal of Applied Polymer Science* **60**, 971-979 (1996).

14. Landin, T. D, Macosko W.C. Cyclization and Reduced Reactivity of Pendant

Vinyls during the Copolymerization of Methyl Methacrylate and Ethylene Glycol Dimethacrylate. *Macromolecules* **21**, 846-851 (1988).

15. Tobita, H. & Hamielec, A.E. Crosslinking kinetics in polyacrylamide networks. *Polymer* **31**, 1546-1552 (1990).

16. Peppas, N.A. & Merrill, E.W. Poly(vinyl-alcohol) hydrogels - reinforcement of radiation-crosslinked networks by crystallization. *Journal of Polymer Science Part A - Polymer Chemistry* **14**, 441-457 (1976).

17. Kim Bumsang, Peppas N.A. Synthesis and characterization of PH-sensitive glycopolymers for oral drug delivery systems. *Journal of Biomater.Sci.Polymer Edn* **13**, 1271-1281 (2002).

18. Lu, S. & Anseth, K.S. Release behavior of high molecular weight solutes from poly(ethylene glycol)-based degradable networks. *Macromolecules* **33**, 2509-2515 (2000).

19. Brahmasandra, S.N., Ugaz, V.M., Burke, D.T., Mastrangelo, C.H. & Burns, M.A. Electrophoresis in microfabricated devices using photopolymerized polyacrylamide gels and electrode-defined sample injection. *Electrophoresis* **22**, 300-311 (2001).

20. Ugaz, V.M., Brahmasandra, S.N., Burke, D.T. & Burns, M.A. Cross-linked polyacrylamide gel electrophoresis of single-stranded DNA for microfabricated

genomic analysis systems. *Electrophoresis* **23**, 1450-1459 (2002).

21. Ugaz, V.M., Burke, D.T. & Burns, M.A. Microdevice-based measurements of diffusion and dispersion in cross-linked and linear polyacrylamide DNA sequencing gels. *Electrophoresis* **23**, 2777-2787 (2002).

22. Ugaz, V.M., Lin, R., Srivastava, N., Burke, D.T. & Burns, M.A. A versatile microfabricated platform for electrophoresis of double- and single-stranded DNA. *Electrophoresis* **24**, 151-157 (2003).

23. Han, J. & Singh, A.K. Rapid protein separations in ultra-short microchannels: Microchip sodium dodecyl sulfate-polyacrylamide gel electrophoresis and isoelectric focusing. *Journal of Chromatography A* **1049**, 205-209 (2004).

24. Song, S., Singh, A.K., Shepodd, T.J. & Kirby, B.J. Microchip dialysis of proteins using in situ photopatterned nanoporous polymer membranes. *Analytical Chemistry* **76**, 2367-2373 (2004).

25. Chen, B. & Chrambach, A. Estimation of polymerization efficiency in the formation of polyacrylamide gel, using continuous optical scanning during polymerization. *Journal of Biochemical and Biophysical Methods* **1**, 105-116 (1979).

26. Giz, A., Catalgil-Giz, H., Alb, A., Brousseau J.L. & Reed, W.F. Kinetics and mechanisms of acrylamide polymerization from absolute, online monitoring of

polymerization reaction. *Macromolecules* **34**, 1180-1191 (2001).

27. Righetti, P.G., Gelfi, C. & Bosisio, A.B. Polymerization kinetics of polyacrylamide gels III. Effect of catalysts. *Electrophoresis* **2**, 291-295 (1981).

28. Gelfi, C., Righetti, P.G. Polymerization kinetics of polyacrylamide gels. *Electrophoresis* **2**, 213-219 (1981).

29. Gelfi C., Righetti, P.G. Polymerization kinetics of polyacrylamide gels II. Effect of temperature. *Electrophoresis* **2**, 220-228 (1981).

30. Okay, O. Kinetic modelling of network formation and properties in free-radical crosslinking copolymerization. *Polymer* **35**, 796-807 (1994).

31. Okay, O. Kinetics of gelation in free radical crosslinking copolymerization. *Polymer* **35**, 2613-2618 (1994).

32. Takata, S.I., Norisuye, T. & Shibayama, M. Preparation temperature dependence and effects of hydrolysis on static inhomogeneities of poly(acrylamide) gels. *Macromolecules* **32**, 3989-3993 (1999).

33. Patras, G., Qiao, G.G. & Solomon, D.H. Controlled formation of microheterogeneous polymer networks: Influence of monomer reactivity on gel structure. *Macromolecules* **34**, 6396-6401 (2001).

34. Kizilay, M.Y. & Okay, O. Effect of initial monomer concentration on spatial inhomogeneity in poly(acrylamide) gels. *Macromolecules* **36**, 6856-6862

(2003).

35. Durmaz, S. & Okay, O. Inhomogeneities in poly(acrylamide) gels: Position-dependent elastic modulus measurements. *Polymer Bulletin* **46**, 409-418 (2001).

36. Kizilay, M.Y. & Okay, O. Effect of swelling on spatial inhomogeneity in poly(acrylamide) gels formed at various monomer concentrations. *Polymer* **45**, 2567-2576 (2004).

37. Anseth, K.S., Bowman, C.N. & Brannon-Peppas, L. Mechanical properties of hydrogels and their experimental determination. *Biomaterials* **17**, 1647-1657 (1996).

38. Klaveness, T.M., Ruoff, P. & Kolnes, J. Kinetics of the cross-linking of poly(acrylamide) with Cr(III). 3. Rheological measurements of the gelation. *Journal of Physical Chemistry* **99**, 8255-8259 (1995).

39. Trompette, J.L., Fabregue, E. & Cassanas, G. Influence of the monomer properties on the rheological behavior of chemically crosslinked hydrogels. *Journal of Polymer Science, Part B: Polymer Physics* **35**, 2535-2541 (1997).

40. Calvet, D., Wong, J.Y. & Giasson, S. Rheological monitoring of polyacrylamide gelation: Importance of cross-link density and temperature. *Macromolecules* **37**, 7762-7771 (2004).

41. Hjerten, S. "Molecular sieve" chromatography on polyacrylamide gels, prepared according to a simplified method. *Arch. Biochem. Biophys.* **1**, 147-151 (1962).

42. Hjerten, S. & Mosbach, R. "Molecular sieve" chromatography of proteins on columns of cross-linked polyacrylamide. *Anal. Biochem.* **3**, 109-118 (1962).

43. Baselga, J., Llorente, M.A., Nieto, J.L., Hernandez-Fuentes, I. & Pierola, I.F. Polyacrylamide network.sequence distribution of crosslinker. *Eur Polym J* **24**, 161-165 (1988).

44. Baselga, J., Hernandez-Fuentes, I., Pierola, I.F. & Llorente, M.A. Elastic properties of highly cross-linked polyacrylamide gels. *Macromolecules* **20**, 3060-3065 (1987).

45. Baselga, J., Llorente, M.A., Hernandez-Fuentes, I. & Pierola, I.F. Network defects in polyacrylamide gels. *European Polymer Journal* **25**, 471-475 (1989).

46. Pascal, P., Napper, D.H., Gilbert, R.G., Pilton, M.C. & Winnik, M.A. Pulsed laser study of the propagation kinetics of acrylamide and methacrylamide in water. *Macromolecules* **23**, 5156-5163 (1990).

47. Pascal, P., Winnik, M.A., Napper, D.H. & Gilbert, R.G. Pulsed laser study of the propagation kinetics of acrylamide and its derivatives in water. *Macromolecules* **26**, 4572-4576 (1993).

48. Kulicke, W.M. & Nottelman, H. Structure and swelling of some synthetic, semisynthetic, and biopolymer hydrogels. *Advanced in Chemistry Series* **223**, 15-44 (1989).

49. Viovy, J.L. Electrophoresis of DNA and other polyelectrolytes: Physical mechanisms. *Reviews of Modern Physics* **72**, 813-872 (2000).

50. Haggerty, L., Sugarman, J.H. & Prud'homme, R.K. Diffusion of polymers through polyacrylamide gels. *Polymer* **29**, 1058-1063 (1988).

51. Hsu, T.-P. & Cohen, C. Observations on the structure of a polyacrylamide gel from electron micrographs. *Polymer* **25**, 1419-1423 (1984).

52. Brahmasandra, S.N., Burke, D.T., Mastrangelo, C.H. & Burns, M.A. Mobility, diffusion and dispersion of single-stranded DNA in sequencing gels. *Electrophoresis* **22**, 1046-1062 (2001).

53. Lo, R.C., Ugaz, V. M. Separation performance of single-stranded DNA electrophoresis in photopolymerized cross-linked polyacrylamide gels. *Electrophoresis* **27**, 373-386 (2006).

54. Agrawal, S. Photoinitiated crosslinked polyacrylamide gels for microdevice electrophoresis. *MS thesis*, Texas A&M University, College Station (2005).

55. Winter, H.H., Mours, M. Rheology of Polymers Near Liquid-Solid Transitions. *Advances in Polymer Science* **134**, 165-234 (1997).

56. Martin E.J., Adolf, D. The sol-gel transition in chemical gels. *Annual review of physical chemistry* **42**, 311-339 (1991).

57. Winter, H.H., Chambon, F. Analysis of Linear Viscoelasticity of a Crosslinking Polymer at the Gel Point. *Journal of Rheology* **30**, 367-382 (1986).

58. Chambon F., Winter, H.H. Linear viscoelasticity at the gel point of a crosslinking PDMS with imbalanced stoichiometry. *Journal of Rheology* **31**, 683-697 (1987).

59. Holly, E.E., Venkataraman S.K., Chambon F., Winter H.H. Fourier tranform mechanical spectroscopy of viscoelastic materials with transient structure *Journal of Non-Newtonian Fhad Mechamcs* **27**, 17-26 (1988).

60. Chambon, F., Petrovic S.Z., Macknight, J. W.,Winter H. H. Rheology of model polyurethanes at gel point. *Macromolecules* **19**, 2146-2149 (1986).

61. Hess, W., Vilgis A.T., Winter H.H. Dynamical critical behavior during chemical gelation and vulcanization. *Macromolecules* **21**, 2536-2542 (1988).

62. Muthukumar, M., Winter, H.H. Fractal dimension of a cross-linking polymer at the gel point. *Macromolecules* **19**, 1284-1285 (1986).

63. Muthukumar, M. Screening effect on viscoelasticity near the gel point. *Macromolecules* **22**, 4658-4660 (1989).

64. Mansur S.H., Orefice L.R., Mansur A.P. Characterization of pol(vinyl

alcohol)/poly(ethylene glycol)hydrogels and PVA-derived hybrids by small-angle X-ray scattering and FTIR spectroscopy. *Polymer* **45**, 7193-7202 (2004).

65. Chambon F., Petrovic S.Z., Macknight J. W.,Winter H.H. Rheology of model polyurethanes at the gel point. *Macromolecules* **19**, 2146-2149 (1986).

66. Izuka A., Winter, H.H., Hashimoto, T. Self-similar relaxation behavior at the gel point of a blend of a cross-linking poly(□-caprolactone) diol with a poly(styrene-co-acrylonitrile). *Macromolecules* **30**, 6158-6165 (1997).

67. Cossar S., Nichetti D., Grizzuti N. A rheological study of the phase transition in the thermoplastic polyurethanes.Critical gel behavior and microstructure development. *Journal of Rheology* **48**, 691-703 (2004).

68. Izuka A., Winter H.H., Hashimoto T. Molecular weight dependence of viscoelasticity of polycaprolactone critical gels. *Macromolecules* **25**, 2422-2428 (1992).

69. Izuka A., Winter H.H., Hashimoto T. Temperature dependence of viscoelasticity of polycaprolactone critical gels. *Macromolecules* **27**, 6883-6888 (1994).

70. Kjøniksen A-L., Nystrom B. Effects of polymer concentration and cross-linking density on rheology of chemically cross-Linked poly(vinyl

alcohol) near the gelation threshold. *Macromolecules* **29**, 5215-5222 (1996).

71. Hernandez, R., Mijangos C., Lopez D. Study of the effect of poly(vinyl alcohol) concentration on the gelation point of poly(vinyl alcohol) poly(acrylic acid) semi-IPN systems as determined by viscoelastic measurements. *Journal of Polymer Science: Part B: Polymer Physics* **43**, 1944-1949 (2005).

72. Payro E.R., Liacuma J.L. Rheological characterizatoion of the gel point in sol-gel transition. *Journal of Non-Crystalline Solids* **352**, 2220-2225 (2006).

73. Liu X., Zhan .G., Yu Y.,Li S. Rheological study on structural transition in polyethersulfone-modified bismaleimide resin during isothermal curing. *Journal of Polymer Science Part B: Polymer Physics* **44**, 3102-3108 (2006).

74. Chambon F., Winter H.H. Stopping of crosslinking reaction in a PDMS polymer at the gel point. *Polymer Bulletin 499-503 (1985)* **13**, 499-503 (1985).

75. Thorgeirsdottir, T.O., Kjøniksen, A.L., Knudsen, K.D., Kristmundsdottir, T. & Nystrom, B. Viscoelastic and structural properties of pharmaceutical hydrogels containing monocaprin. *European Journal of Pharmaceutics and Biopharmaceutics* **59**, 333-342 (2005).

76. Wang, J., Ugaz, V.M. Using in situ rheology to characterize the microstructure in photopolymerized polyacrylarnide gels for DNA electrophoresis. *Electrophoresis* **27**, 3349-3358 (2006).

77. Izuka, A., Winter, H.H., Hashimoto T. Self-Similar relaxation behavior at the gel Point of a blend of a cross-linking poly(-caprolactone) diol with a poly(styrene-co-acrylonitrile). *Macromolecules* **30**, 6158-6165 (1997).

78. Scanlan, C.J., Winter H.H. Composition dependence of the viscoelasticity of end-linked poly(dimethylsi1oxane) at the gel point. *Macromolecules* **24** (1991).

79. Peppas, N.A. & Barr-Howell, B.D. in Hydrogels in Medicine and Pharmacy. (ed. N.A. Peppas) 27-56 (CRC Press, Boca Raton; 1986).

80. Bray, J.C., Merrill E.W. Poly (vinyl alcohol) hydrogels formation by electron beam irradiation of aqueous solutions and subsequent crystallization. *Journal of Applied Polymer Science* **17**, 3779-3794 (1973).

81. Canal, T., Peppas N.A. Correlation between mesh size and equilibrium degree of swelling of polymeric networks. *Journal of Biomedical Materials Research* **23**, 1183-1193 (1989).

82. Flory, P.J. Principles of Polymer Chemistry. (Cornell University Press, Ithaca, NY; 1953).

83. Martens, P., Anseth K.S. Characterization of hydrogels formed from acrylate modified poly(vinyl alcohol) macromers. *Polymer* **41**, 7715-7722 (2000).

84. Anseth, K.S., Bowman, C.N. & Brannon-Peppas, L. Mechanical properties of hydrogels and their experimental determination. *Biomaterials* **17**, 1647-1657

(1996).

85. Bryant, S.J. & Anseth, K.S. in Scaffolding in Tissue Engineering. (eds. P.X. Ma & J. Elisseeff) 71-90 (CRC Press, Boca Raton; 2006).

86. Cohen, Y., Ramon, O., Kopelman, I.J. & Mizrahi, S. Characterization of inhomogeneous polyacrylamide hydrogels. *Journal of Polymer Science Part B: Polymer Physics* **30**, 1055-1067 (1992).

87. Nishio, I., Reina, J.C.,Bansil, R. Quasielastic light-scattering study of the movement of particles in gels *Physical Review Letters* **59**, 684-687 (1987).

88. Chui, M.M., Phillips, R.J. & Mccarthy, M.J. Measurement of the porous microstructure of hydrogels by nuclear-magnetic-resonance. *Journal of Colloid and Interface Science* **174**, 336-344 (1995).

89. Kim, S.H. & Chu, C.C. Pore structure analysis of swollen dextran-methacrylate hydrogels by SEM and mercury intrusion porosimetry. *Journal of Biomedical Materials Research* **53**, 258-266 (2000).

90. Maaloum, M., Pernodet, N. & Tinland, B. Agarose gel structure using atomic force microscopy: Gel concentration and ionic strength effects. *Electrophoresis* **19**, 1606-1610 (1998).

91. Pernodet, N., Maaloum, M. & Tinland, B. Pore size of agarose gels by atomic force microscopy. *Electrophoresis* **18**, 55-58 (1997).

92. Sun Guoming, Chu, C-C. Synthesis, characterization of biodegradable dextran–allyl isocyanate–ethylamine/polyethylene glycol–diacrylate hydrogels and their in vitro release of albumin. *Carbohydrate Polymers* **65**, 273–287 (2006).

93. Rüchel, R., Steere, R.L., Erbe, E.F. Transmission-electron microscopic observations of freeze-etched polyacrylamide gels. *Journal of Chromatography* **166**, 563-575 (1978).

94. Hawkins, D.M., Ellis, E.A., Stevenson, D., Holzenburg, A. & Reddy, S.M. Novel critical point drying (CPD) based preparation and transmision electron microscopy (TEM) imaging of protein specific molecularly imprinted polymers (HydroMIPs). *Journal of Materials Science* **42**, 9465-9468 (2007).

95. Brun, M., Lallemand, A., Quinson, J-F., Eyraud, C. A new method for the simultaneous determination of the size and shape of pores: the thermoporometry. *Thermochimica Acta* **21**, 59-88 (1977).

96. Defay R., Prigogine, I., Bellemans, A. Surface Tension and Adsorption. (Wiley, New York; 1966).

97. Landry, M.R. Thermoporometry by differential scanning calorimetry:experimental considerations and applications. *Thermochimica Acta* **433**, 27-50 (2005).

98. Ishikiriyama, K. & Todoki, M. Pore size distribution measurements of silica gels by means of differential scanning calorimetry: II. Thermoporosimetry. *Journal of Colloid and Interface Science* **171**, 103-111 (1995).

99. Ishikiriyama, K., Todoki, M. & Motomura, K. Pore size distribution (PSD) measurements of silica gels by means of differential scanning calorimetry. *Journal of Colloid and Interface Science* **171**, 92-102 (1995).

100. Landry, M.R. Thermoporometry by differential scanning calorimetry: experimental considerations and applications. *Thermochimica Acta* **433**, 27-50 (2005).

101. Boontheekul, T., Kong, H.-J. & Mooney, D.J. Controlling alginate gel degradation utilizing partial oxidation and bimodal molecular weight distribution. *Biomaterials* **26**, 2455-2465 (2005).

102. Iza, M., Woerly, S., Danumah, C., Kaliaguine, S. & Bousmina, M. Determination of pore size distribution for mesoporous materials and polymeric gels by means of DSC measurements: thermoporometry. *Polymer* **41**, 5885-5893 (2000).

103. Quicke, D.L.J., Belshaw, R. & Lopez-Vaamonde, C. Preservation of hymenopteran specimens for subsequent molecular and morphological study. *Zoologica Scripta* **28**, 261-267 (1999).

104. Williams B.David, C.B.C. Transmission electron microscopy : a textbook for materials science. (Plenum Press, New York 1996).

105. Lo, R.C. & Ugaz, V.M. Separation performance of single-stranded DNA electrophoresis in photopolymerized crosslinked polyacrylamide gels. *Electrophoresis* **27**, 373-386 (2006).

106. Stellwagen, N.C. Apparent pore size of polyacrylamide gels: Comparison of gels cast and run in Tris-acetate-EDTA and Tris-borate-EDTA buffers. *Electrophoresis* **19**, 1542-1547 (1998).

107. Yamamoto T., Endo, A., Inagi Y., Ohmori T., Nakaiwa M. Evaluation of thermoporometry for characterization of mesoporous materials. *Journal of Colloid and Interface Science* **284**, 614-620 (2005).

108. Hay N.J., Laity, R.P. Observations of water migration during thermoporometry studies of cellulose films. *Polymer* **2000**, 6171-6180 (2000).

109. Iza, M., Woerly S., Danumah C., Kaliaguine, S.& Bousmina, M. Determination of pore size distribution for mesoporous materials and polymeric gels by means of DSC measurements: thermoporometry. *Polymer* **41**, 5885-5893 (2000).

110. Yamamoto T., Mukai, R.S., Nitta K.,Tamon H.,Endo A.,Ohmori T.,Nakaiwa M. Evaluation of porous structure of resorcinol-formaldehyde hydrogels by thermoporometry. *Thermochimica Acta* **439**, 74-79 (2005).

111. Kopecka, K., Drouin, G. & Slater, G.W. Capillary electrophoresis sequencing of small ssDNA molecules versus the Ogston regime: Fitting data and interpreting parameters. *Electrophoresis* **25**, 2177-2185 (2004).

112. Chang, Y. & Allcock, H. Synthesis and characterization of covalently interconnected phosphazene-silicate hybrid network membranes. *Chemistry of Materials* **17**, 4449-4454 (2005).

113. Tsunomori, F. & Ushiki, H. Pore size effect on diffusion coefficient of rhodamine B in PNIPA gel. *Physics Letters A* **258**, 171-176 (1999).

VITA

Jian Wang received his Bachelor of Science degree in chemical engineering from China University of Petroleum (Beijing) in 1996. He entered the chemical engineering program at the Research Institute of Petroleum Processing (China) and received his Master of Science degree in March 2002. He entered the graduate school in Texas A&M University and received his Ph.D. in chemical engineering in May 2008. His research interest includes polymer, rheology and catalysis.

Dr. Jian Wang may be reached at Department of Chemical Engineering, Texas A&M University, College Station, Texas, 77840-3122. His E-mail is wjtwin@gmail.com.